Monthly Notices of the ROYAL ASTRONOMICAL SOCIETY

MNRAS **536,** 664–683 (2025) https://doi.org/10.1093/mnras/stae2562
Advance Access publication 2024 November 18

Matter power spectra in modified gravity: a comparative study of approximations and *N*-body simulations

B. Bose [1,2★] A. Sen Gupta,[3,4] B. Fiorini,[4] G. Brando,[5] F. Hassani,[6] T. Baker,[4] L. Lombriser,[7] B. Li [8] C. Ruan,[6] C. Hernández-Aguayo [9,10] L. Atayde[11] and N. Frusciante[12]

[1]*Institute for Astronomy, University of Edinburgh, Royal Observatory, Blackford Hill, Edinburgh EH9 3HJ, UK*
[2]*Basic Research Community for Physics e.V., Veddeler Brückenstrasse, 122 20539 Hamburg , Germany*
[3]*Astronomy Unit, School of Physical and Chemical Sciences, Queen Mary University of London, Mile End Road, London E1 4NS, UK*
[4]*Institute of Cosmology and Gravitation, University of Portsmouth, Burnaby Road, Portsmouth PO1 3FX, UK*
[5]*Max Planck Institute for Gravitational Physics (Albert Einstein Institute) Am Mühlenberg 1, D-14476 Potsdam-Golm, Germany*
[6]*Institute of Theoretical Astrophysics, University of Oslo, P.O. Box 1029 Blindern, 0315 Oslo, Norway*
[7]*Département de Physique Théorique, Université de Genève, 24 quai Ernest Ansermet, CH-1211 Genève 4, Switzerland*
[8]*Institute for Computational Cosmology, Department of Physics, Durham University, South Road, Durham DH1 3LE, UK*
[9]*Max-Planck-Institut für Astrophysik, Karl-Schwarzschild-Str. 1, D-85748 Garching, Germany*
[10]*Excellence Cluster ORIGINS, Boltzmannstrasse 2, D-85748 Garching, Germany*
[11]*Instituto de Astrofisíca e Ciências do Espaço, Faculdade de Ciências da Universidade de Lisboa, Edificio C8, Campo Grande, P-1749016 Lisboa, Portugal*
[12]*Dipartimento di Fisica 'E. Pancini', Università degli Studi di Napoli 'Federico II', Compl. Univ. di Monte S. Angelo, Edificio G, Via Cinthia, I-80126 Napoli, Italy*

Accepted 2024 November 4. Received 2024 October 15; in original form 2024 June 27

ABSTRACT

Testing gravity and the concordance model of cosmology, ΛCDM, at large scales is a key goal of this decade's largest galaxy surveys. Here we present a comparative study of dark matter power spectrum predictions from different numerical codes in the context of three popular theories of gravity that induce scale-independent modifications to the linear growth of structure: nDGP, Cubic Galileon, and K-mouflage. In particular, we compare the predictions from *N*-body simulations solving the full scalar field equation, two *N*-body codes with approximate time integration schemes, a parametrized modified *N*-body implementation, and the analytic halo model reaction approach. We find the modification to the ΛCDM spectrum is in 2 per cent agreement at $z \leq 1$ and $k \leq 1\ h\,\mathrm{Mpc}^{-1}$ over all gravitational models and codes, in accordance with many previous studies, indicating these modelling approaches are robust enough to be used in forthcoming survey analyses under appropriate scale cuts. We further make public the new code implementations presented, specifically the halo model reaction K-mouflage implementation and the relativistic Cubic Galileon implementation.

Key words: methods: numerical – cosmology: large-scale structure of Universe – cosmology: theory.

1 INTRODUCTION

Observations of cosmological large-scale structure (LSS) offer a unique laboratory in which to test the concordance cosmological model, ΛCDM, which assumes General Relativity (GR). Such experiments are highly motivated. Indeed, the nature of the cold dark matter (CDM) and the constant dark energy (Λ) components, constituting 95 per cent of the Universe's total energy density (see for example Riess et al. 1998; Perlmutter et al. 1999; Aghanim et al. 2020; Alam et al. 2021), remains elusive. Moreover, ΛCDM's inability to reconcile principles of GR with quantum mechanics points to the need for a more unified theory (see Bernardo et al. 2022, for a recent review on gravitational approaches to the cosmological constant problem). These gaps in our understanding motivate the investigation into alternative theories beyond ΛCDM. By exploring these new frontiers, we hope to uncover a more comprehensive picture of the Universe, potentially leading to groundbreaking insights into its origin, evolution, and ultimate fate.

This decade will provide an immense opportunity for such insights through the efforts of some of the biggest scientific collaborations to date. These include the European Space Agency's *Euclid* mission (Barroso et al. 2024), the Vera Rubin Observatory (LSST Dark Energy Science Collaboration 2012, ; Ivezić et al. 2019) (LSST),[1] the Dark Energy Survey (Albrecht et al. 2006; Abbott et al. 2016), the *Nancy Grace Roman Space Telescope* (Akeson et al. 2019), and the Dark Energy Spectroscopic Instrument (Levi et al. 2019,). For instance, *Euclid* and LSST will be measuring up to order 1 billion galaxy shapes (Ivezić et al. 2019; Barroso et al. 2024), 2 orders of magnitude more than previous surveys (see for example Hildebrandt et al. 2017). This means the statistical precision of its resulting weak

★ E-mail: ben.bose@ed.ac.uk

[1] Vera Rubin was formerly known as the Large Synoptic Survey Telescope.

lensing measurements, such as cosmic shear, will be roughly the same order of magnitude better than previous observations, providing a potentially brilliant probe for new physics.

Consistency tests of ΛCDM are a primary goal, but these missions are also charged with investigating if there is any statistical preference for new physics. Such beyond-consistency tests require theoretical modelling of any new physics we wish to test. In particular, a key task is to theoretically model key statistical cosmological quantities over a very wide range of physical scales. The 2-point correlation function, or its Fourier analogue, the power spectrum, of the cosmological matter distribution is one such summary statistic. At small physical scales, where we have many more galaxy pairs, the measured statistics will be far more precise, potentially providing a heightened signal of any new physics. It is thus imperative to model these scales accurately. It should be kept in mind that this work only considers the matter power spectrum, which is a key ingredient for cosmic shear weak lensing analyses.

The small scale precision measurements of forthcoming surveys has forced ambitious accuracy demands on such theoretical predictions (for example $\mathcal{O}(1$ per cent) accuracy on the matter power spectrum; Hearin, Zentner & Ma 2012; Ivezić et al. 2019; Martinelli et al. 2021). These accuracy demands are tied to the imposition of scale cuts, which limit the non-linear data that can be used in analyses. Most *Euclid* forecasts (Blanchard et al. 2020; Bonici et al. 2023; Casas et al. 2023; Frusciante et al. 2024) consider a 'pessimistic' and 'optimistic' scale cut in harmonic space, corresponding to a maximum angular multipole of $\ell = 1500$ and $\ell = 5000$, with the precise value of these cuts in Fourier mode, or k-space, varying with redshift. In contrast, LSST applies scale cuts in real space. In practice such cuts should be inferred by performing extensive mock parameter inference analyses and quantifying the bias accrued by using increasingly non-linear data. In this way, accuracy demands in k-space say, serve as a rough guide to ensure the safe usage of the data up to a given scale in forthcoming analyses.

For these reasons, the community has sought to accurately model these small, non-linear scales in the matter power spectrum, for beyond-ΛCDM scenarios. To this end, many methods have been developed to provide such predictions. N-body simulations provide our most accurate predictions, and have been extended to many models beyond-ΛCDM (see for example Li et al. 2012; Puchwein, Baldi & Springel 2013; Li, Zhao & Koyama 2013a; Li et al. 2013b; Llinares, Mota & Winther 2014; Hassani et al. 2019, 2020; Hernández-Aguayo et al. 2022; Ruan et al. 2022; Christiansen et al. 2023). This accuracy comes at a large computational cost, making this method inappropriate for expensive data-theory comparisons where we wish to sample a large cosmological and gravitational parameter space. One can alleviate this cost to some extent through approximate methods. For example, Comoving Lagrangian Acceleration (COLA) (Tassev, Zaldarriaga & Eisenstein 2013; Howlett, Manera & Percival 2015) is an N-body method that provides a balance between accuracy and speed by reducing the time-steps in particle evolution through the perturbative modelling of large-scale physics. This method has also been extended to many alternatives to ΛCDM (Winther et al. 2017; Brando, Koyama & Winther 2023; Wright et al. 2023).

While being faster, COLA methods are still too slow to use directly in data analyses. Despite the computational cost, simulation methods are essential in bench-marking or constructing faster predictive pipelines, such as emulators (Ramachandra et al. 2021; Arnold et al. 2022; Harnois-Déraps et al. 2023; Fiorini, Koyama & Baker 2023; Nouri-Zonoz, Hassani and Kunz 2024) or analytic models (Zhao 2014; Mead et al. 2016). The halo model reaction (Cataneo et al. 2019) is one such analytic method, which can provide a high accuracy at a fraction of the time cost and is theoretically general, allowing its extension to many models of cosmology.

This paper is dedicated to assessing the consistency of these different methods for a few representative beyond-ΛCDM models of cosmological relevance. The models we consider are the DGP braneworld model (Dvali, Gabadadze & Porrati 2000), the Cubic Galileon model (Nicolis, Rattazzi & Trincherini 2009), and the K-mouflage model (Babichev, Deffayet & Ziour 2009). This work runs in a similar vein to the code comparison projects of Ref. Winther et al. (2015), updating the exercise, nearly a decade later, to account for improvements in the codes and methods, as well as approximations and new theoretical models and phenomenology.[2] Such an assessment is vital in modelling the theoretical uncertainty or delimiting the scales of validity of the method under consideration, which will play an important role in forthcoming surveys (Audren et al. 2013; Baldauf et al. 2016). We also present an extension of the halo model reaction code, `react`, which includes the specific K-mouflage model of gravity considered in this paper.

We outline the paper as follows: In Section 2 we briefly introduce the different beyond-ΛCDM models we consider. In Section 3 we outline the different methods we will compare, highlighting the key differences between them and the various approximations they employ. In Section 4 we present matter power spectrum boost comparisons of the different methods. We present our conclusions in Section 5.

1.1 Notation and conventions

In this work we will use the following definitions and conventions:

(i) We use a metric signature of $(-, +, +, +)$.
(ii) We work in units where $c = \hbar = 1$.
(iii) Jordan frame quantities appear with a hat, e.g. $\hat{q}$.
(iv) The Planck mass is denoted as $M_{\rm pl} = (8\pi G_{\rm N})^{-1}$, where $G_{\rm N}$ is Newton's constant.
(v) Overdots denote derivatives with respect to cosmic time t.
(vi) Primes denote derivatives with respect to the natural logarithm of the scale factor, $\ln a$, unless otherwise stated.
(vii) Quantities with a '0' subscript denote their value at $z = 0$.
(viii) The canonical scalar field kinetic energy is $X \equiv -(\partial\phi)^2/2$.

2 GRAVITY BEYOND GENERAL RELATIVITY

The simplest, viable class of alternatives to ΛCDM can be found by adding a single extra scalar degree of freedom, ϕ, to GR. Under some basic constraints, such as second-order equations of motion (a generic condition to avoid unbounded negative energies) and four space–time dimensions, the well-studied Horndeski Lagrangian encompasses all possible scalar–tensor theories with minimally coupled matter (Horndeski 1974; Deffayet et al. 2011; Kobayashi 2019). If we accept the speed of light to be the same as gravitational wave propagation, in accordance with the observation of gamma-ray burst GRB 170817A (Goldstein et al. 2017) and merger signal of GW170817 (Abbott et al. 2017), the Horndeski Lagrangian reduces to,[3] (Lombriser & Taylor

[2]For a similar recent exercise see Ref. Adamek et al. (2024).
[3]This condition may not hold below the frequency band of terrestrial gravitational wave detectors (de Rham & Melville 2018; de Rham, Melville & Noller 2021; Baker et al. 2022; Harry & Noller 2022; Baker et al. 2023). Further, it should be noted that equation (1) is not the most general action describing theories that do not violate the results of GW170817. Some Gauss–Bonet theories are excluded, for example; see Ref. Clifton et al. (2020).

2016; Baker et al. 2017; Creminelli & Vernizzi 2017; Ezquiaga & Zumalacárregui 2017; Lombriser & Lima 2017; Sakstein & Jain 2017; Battye, Pace & Trinh 2018; Creminelli et al. 2018; Rham & Melville 2018; Quartin et al. 2023)

$$\mathcal{L}_{\rm H} = G_4(\phi)\, R + G_2(\phi, X) - G_3(\phi, X)\Box\phi\,, \tag{1}$$

where R is the Ricci curvature scalar, $\Box$ is the D'Alembert operator, and each $G_i(\phi, X)$, $i = 2, 3, 4$ is a free function of the scalar field ϕ and its canonical kinetic term X. Note that the G_4 operator is a function of ϕ only.

Besides modifying the expansion history of the Universe, modified gravity theories also leave an impact on the growth of structure (see Hou et al. 2023, for a review). This is generally understood by considering linear perturbations on top of a homogeneous and isotropic Friedmann–Lemaître–Robertson–Walker background given by the following line element

$$\mathrm{d}s^2 = -(1+2\Psi)\,\mathrm{d}t^2 + a^2(t)\,(1-2\Phi)\,\boldsymbol{\delta}_{ij}\mathrm{d}x^i\mathrm{d}x^j\,, \tag{2}$$

where Φ is the usual Poisson potential in Newtonian gravity that captures perturbations in the spatial sector of the metric, while Ψ is a gravitational potential corresponding to perturbations in the time-like sector of the line element.

The linear evolution of perturbations of modified gravity theories given by equation (1) has been thoroughly studied by many different works in the literature (see for example Hu et al. 2014; Zumalacárregui et al. 2017; Frusciante & Perenon 2020). Within the quasi-static approximation (Sawicki & Bellini 2015; Winther & Ferreira 2015b; Pace et al. 2021), the effects of modified gravity on the linear growth of structure in the Universe are encoded in a time- and scale-dependent effective gravitational constant

$$G_{\rm eff,L}(k, a) = G_{\rm N}\left[1 + \frac{\Delta G_{\rm eff,L}(k, a)}{G_N}\right], \tag{3}$$

where k is the Fourier mode. In this work, we only consider theories where the linear modification is scale-independent and so we drop the dependence on k for $G_{\rm eff,L}$, where L refers to a linear theory prediction. The Poisson equation at large scales is then written in Fourier space as

$$k^2\Phi(k, a) = 4\pi\, G_{\rm eff,L}(a) a^2 \bar{\rho}_{\rm m}(a)\delta_{\rm m}(k, a), \tag{4}$$

where $\bar{\rho}_{\rm m}$ is the background matter density, and $\delta_{\rm m}$ is the corresponding linear matter perturbation.

Another requirement for this class of theories is the inclusion of a theoretical mechanism that prevents large modifications in environments where GR-like physics has been well confirmed by experiment (see Will 2014; Belgacem et al. 2019, for example). Such mechanisms are known as screening mechanisms (see Brax et al. 2021, for a recent review and experimental tests). The screened environments are small scale, dense environments. This means that the modification to Newton's constant, more generally written as

$$G_{\rm eff}(k, a) = G_{\rm N}\left[1 + \frac{\Delta G_{\rm eff}(k, a)}{G_N}\right], \tag{5}$$

requires the condition that $\lim_{k\to\infty} G_{\rm eff}(k, a) \to G_{\rm N}$. In this case $G_{\rm eff}(k, a)$ is the effective gravitational constant valid at all scales – both linear and non-linear – and it necessarily depends on scale as well as time. In this work we will meet two such screening mechanisms which satisfy this condition: the Vainshtein mechanism and K-mouflage screening.

Returning to equation (1), we will consider three choices for the Lagrangian functions, each having very particular phenomenological features, including different screening mechanisms and cosmological backgrounds. Where a choice exists, we will give their Lagrangians in the Einstein frame where $G_4(\phi) = M_{\rm pl}^2/2$, with metric $\boldsymbol{g}_{\mu\nu}$. In this frame the 'pure gravity' part of the action resembles the Einstein–Hilbert action for GR, simplifying some computations. However, this frame choice also results in non-minimal coupling of matter to the metric, ensuring the theory behaves very differently to GR.

The Einstein frame is obtained by performing a conformal transformation of the Jordan frame. The Jordan frame prioritizes use of a metric, $\hat{g}_{\mu\nu}$, which couples minimally to the matter fields but contains the non-trivial G_4 function, departing from the the Einstein–Hilbert action. The Jordan-frame metric is related to the Einstein-frame metric, $\boldsymbol{g}_{\mu\nu}$, via a conformal factor A that is a function of the Horndeski scalar:

$$\hat{\boldsymbol{g}}_{\mu\nu} = A^2(\phi)\boldsymbol{g}_{\mu\nu}\,. \tag{6}$$

In what follows, specifically in the case of K-mouflage theories, we will see that some quantities differ between the Jordan and Einstein frame. Though these quantities may be 'physical' in nature, they are not directly observable. General coordinate invariance – a key property shared with GR by nearly all modified gravity theories – ensures that observable quantities must be independent of frame choices (see for example Catena, Pietroni & Scarabello 2007; Chiba & Yamaguchi 2013; Francfort, Ghosh & Durrer 2019).

We summarize the models considered in this paper, their associated additional parameters, and some selected constraints in Table 1.

2.1 nDGP

The first model we consider is the Dvali–Gabadadze–Porrati model (Dvali et al. 2000), which does not strictly fall into the Horndeski class, being a 5D braneworld model. It is given by the following action

$$S = \frac{1}{16\pi G_5}\int_{\mathcal{M}} \mathrm{d}^5x\sqrt{-\gamma}R_5 + \int_{\partial\mathcal{M}} \mathrm{d}^4x\sqrt{-g}\left[\frac{M_{\rm pl}^2}{2}R + \mathcal{L}_{\rm m}\right], \tag{7}$$

where γ is the 5D metric and R_5 its Ricci curvature scalar. G_5 is the 5D gravitational constant. The matter Lagrangian is restricted to a 4D brane in a 5D Minkowski space–time. The induced gravity given by the 4D Einstein–Hilbert action is responsible for the recovery of 4D gravity on the brane. The parameter $r_{\rm c} = G_5/(2G_{\rm N})$ is called the cross-over scale and is the only free parameter of the model, with its GR limit being $r_{\rm c} \to \infty$.

DGP also exhibits screening coming from higher order derivative terms in the effective 4D action. Such screening is known as Vainshtein screening (Vainshtein 1972; Babichev & Deffayet 2013). The so-called decoupling limit of DGP has the effective action given by (Luty, Porrati & Rattazzi 2003; Gabadadze & Iglesias 2006; Jain & Khoury 2010)

$$\mathcal{L}_{\rm DGP} = \frac{M_{\rm pl}^2}{2}R + \left(3\phi - \frac{1}{\Lambda_{\rm DGP}^3}(\partial\phi)^2\right)\Box\phi + \frac{1}{2M_{\rm pl}^2}\phi T\,, \tag{8}$$

where T is the trace of the energy momentum tensor and $\Lambda_{\rm DGP}^3 = M_{\rm pl}^2/r_c^2$. Note that although equation (7) is not a Horndeski Lagrangian, equation (8) is (compare to equation 1). In this case we have

$$G_3(\phi, X) = 3\phi + \frac{2}{\Lambda_{\rm DGP}^3}X\,, \tag{9}$$

with $G_2(\phi, X) = 0$ and $G_4(\phi) = M_{\rm pl}^2/2$.

Table 1. Overview of gravity models considered in this work. Note the K-mouflage kinetic term in equation (14) does not pass Solar System tests without running into fine-tuning issues (Barreira et al. 2015b). Note the CG has no free parameters with the tracker solution. We have included constraints for the more general GCCG (see Section 2.2).

Model	Screening method	Free parameters	Selected data constraints
nDGP	Vainshtein	$\{\Omega_{\rm rc}\}$	$\Omega_{\rm rc} \leq 0.235\,(2\sigma)$ (LSS) (Barreira, Sánchez & Schmidt 2016)
CG	Vainshtein	$\{s = 2, q = 0.5\}$	$s = 0.05^{+0.08}_{-0.05}$, $q > 0.8(2\sigma)$ (Various LSS, GCCG) (Frusciante et al. 2020)
K-mouflage	K-mouflage	$\{n, \beta_{\rm K}, K_0, \lambda\}$	$\beta_{\rm K} \leq 0.1$ (Lunar laser ranging) (Barreira et al. 2015b)

The literature typically assumes a ΛCDM background expansion for this model, which is accommodated by introducing an appropriate dark energy contribution (see for example Schmidt 2009b; Bag, Mishra & Sahni 2018) on the stable 'normal' branch solution of the Friedmann equations. We follow this here (see Lue 2006, for more details) and refer to this normal branch as nDGP. We also parametrize the modification to gravity using the energy density fraction $\Omega_{\rm rc} \equiv 1/(4r_{\rm c}^2 H_0^2)$, where H_0 is the Hubble constant. The GR-limit is then $\Omega_{\rm rc} \to 0$.

Although nDGP is now quite strongly constrained by observations (see for example Lombriser et al. 2009; Barreira et al. 2016; Piga et al. 2023), its appeal as a modified gravity model stems from the simplicity of its 4D effective action relative to the new phenomenology it introduces. It is one of the simplest examples of a gravity model that produces Vainshtein screening effects, whilst maintaining scale-independent growth of matter perturbations, and having only one additional parameter relative to ΛCDM. This has made it a favourite testbed for simulations (Khoury & Wyman 2009; Schmidt 2009a; Li et al. 2013a; Winther et al. 2017) and analyses with galaxy surveys (Barreira et al. 2016; Piga et al. 2023; Frusciante et al. 2024). We refer the reader to Refs. Koyama & Maartens (2006); Li et al. (2013a), and Section B for details on the modification to the Poisson equation (equation 4) in linear and non-linear regimes.

2.2 Cubic Galileon

The Cubic Galileon (CG) model was first derived by Nicolis et al. (2009) as a generalization of the effective DGP action in 4D. The Lagrangian is given by (see for example Deffayet, Esposito-Farese & Vikman 2009; Kobayashi, Yamaguchi & Yokoyama 2010)

$$\mathcal{L}_{\rm CG} = R\frac{M_{\rm pl}^2}{2} + c_2 X + \frac{1}{\Lambda_3^3} c_3 X \Box\phi\,, \tag{10}$$

where c_2 and c_3 are dimension-less constants parametrizing the modification to gravity, and the canonical choice for Λ_3 being $\Lambda_3^3 = M_{\rm pl} H_0^2$, made to give the scalar field non-trivial dynamics on cosmological scales. Comparing with equation (1) we have

$$G_2(\phi, X) = c_2 X\,, \qquad G_3(\phi, X) = -\frac{1}{M_{\rm pl} H_0^2} c_3 X\,. \tag{11}$$

This model also exhibits the Vainshtein mechanism due to the presence of the higher order derivative terms (see Barreira et al. 2013a, for a derivation in the case of spherical symmetry). In this model, $G_4(\phi) = A(\phi)^{-2}/2 = 1$, and hence there is no difference between Jordan and Einstein frames (see equation 6). We note that the absence of G_4 and conformal coupling allows one to interpret this model as a dark energy model with a non-trivial kinetic term.

The Cubic Galileon model is one member of a broader family, the Galileons, which add further derivative terms to equation (10) (Deffayet et al. 2009). The Galileon family received intense interest from the theoretical physics community due to their shift symmetry properties (the actions are invariant under a shift $\phi(x) \to \phi(x) + c + \boldsymbol{b}_\mu \boldsymbol{x}^\mu$, c and $\boldsymbol{b}_\mu$ constants); this leads to special properties of the S-matrix. Cosmologically, their impact has been studied on the CMB (for example Barreira et al. 2014; Peirone et al. 2019; Frusciante et al. 2020; Albuquerque, Frusciante & Martinelli 2022), linear matter power spectrum (for example Barreira et al. 2012) and gravitational lensing by voids (for example Baker et al. 2018). See also Refs. Renk et al. (2017), Peirone et al. (2018), and Frusciante & Pace (2020) for other observational implications.

The more complex Galileon siblings have been virtually eliminated by their inability to have gravitational waves propagate at the speed of light, leaving behind only the CG (see for example Baker et al. 2017; Ezquiaga & Zumalacárregui 2017). The CG model can be constrained by considering the integrated Sachs–Wolfe effect cross-correlated with a galaxy sample, as was done in Refs. Renk et al. (2017) and Kable et al. (2022). The resulting cross-correlation, however, is shown to be anticorrelated with the expected ΛCDM signal, which severely constrains this model. It is worth noting, nevertheless, that a broader class of cubic Horndeski theories does not show this anticorrelation (Brando et al. 2019).

Similarly to nDGP, it remains a useful testbed displaying Vainshtein screening, with a larger degree of flexibility due to its additional parameters and energy scales. We also note that the non-zero G_2 term makes this model phenomenologically distinct from nDGP. Further, in this paper we do not assume a ΛCDM background as with nDGP, but rather the solution to the Friedmann equations which include the effects of the scalar field (see for example Barreira et al. 2013a). A cosmology with this background evolution but with no further gravitational modification (so the Poisson equation remains as in GR), will be referred to as QCDM as in Ref. Barreira et al. (2013a).

The more general Generalized Covariant Cubic Galileon (GCCG) was recently considered in Ref. Frusciante et al. (2020), which promotes the G_i functions to be power-law functions of X, i.e. $G_i \propto X^{p_i}$. This model permits a tracker solution at the background level which is given by (De Felice & Tsujikawa 2012)

$$H^{2q+1}\psi^{2q} = \zeta H_0^{2q+1}\,, \tag{12}$$

where $q \equiv (p_3 - p_2) + 1/2$ and $\psi = \phi'/M_{\rm pl}$. We also have the parameter $s = p_2/q$, leaving only two additional degrees of freedom for this model over ΛCDM. The GCCG reverts to the CG model when $q = 0.5$ and $s = 2$.

The GCCG model has not been ruled out by data, with CMB experiments giving the 2σ bounds of $q > 0$ and $s = 0.6^{+1.7}_{-0.6}$, with a slight preference for the model over ΛCDM (Frusciante et al. 2020). When combined with SN1a and redshift space distortion data sets, the bounds improve to $q > 0.8$ and $s = 0.05^{+0.08}_{-0.05}$. We note that theoretical stability conditions require both parameters to be positive.

In this paper we will only consider the CG limit of GCCG. We note that we employ the GCCG patch to the `react` code (Atayde et al. 2024) for those specific predictions. For details on how the

Poisson equation is modified in the CG limit, we refer the reader to Refs. Barreira et al. (2013a) and Atayde et al. (2024).

2.3 K-mouflage

2.3.1 Lagrangian

The last model we consider is the K-mouflage model (Babichev et al. 2009). This model has the Lagrangian (in the Einstein frame)

$$\mathcal{L}_{\rm K} = R\frac{M_{\rm pl}^2}{2} + \mathcal{M}^4 K(X)\,, \tag{13}$$

where $K(X)$ is a function of the canonical kinetic term, equivalent to a restricted $G_2(\phi, X)$, and $\mathcal{M}^4$ is an energy scale of the theory.[4] We will set $\mathcal{M}^4 = \lambda^2 H_0^2 M_{\rm pl}^2$ as in Ref. Hernández-Aguayo et al. (2022), λ being an order 1 dimension-less constant which can be tuned to give the current accelerated expansion of the Universe today. In this work we will consider a form which has been well studied in the literature (Brax & Valageas 2014a, b; Barreira et al. 2015a, b; Hernández-Aguayo et al. 2022)

$$K(X) = -1 + \frac{1}{H_0^2\lambda^2 M_{\rm pl}^2}X + K_0\frac{1}{H_0^{2n}\lambda^{2n}M_{\rm pl}^{2n}}X^n\,, \tag{14}$$

where K_0 is another dimension-less model parameter and $n \geq 2$ is an integer. For the conformal function, we assume an exponential form

$$A(\phi) = \exp\left(\frac{\beta_{\rm K}\phi}{M_{\rm pl}}\right)\,, \tag{15}$$

where $\beta_{\rm K}$ is another dimension-less model parameter. In total we then have four parameters for this particular model: $\{\lambda, K_0, n, \beta_{\rm K}\}$.

Unlike the other two models considered, the Jordan and Einstein frames are not set to be identical ($A(\phi) \neq 1$) which distinguishes this model from k-essence theories (Armendariz-Picon, Damour & Mukhanov 1999) where a universal coupling to matter is not present. In this work we will develop predictions for both frames. We provide the transformations of key quantities in the next subsection.

This model exhibits a similar screening mechanism to Vainshtein screening, although quantitatively different due to the absence of the higher order $G_3(\phi, X)\Box\phi$ term, giving it a unique phenomenology. In particular, in dense environments of mass m, the K-mouflage radius – the scale below which GR is recovered – goes as $m^{1/2}$, whereas in Vainshtein theories this screening occurs at smaller scales, with a dependence of the Vainshtein radius on the environmental mass being $m^{1/3}$ (Brax & Valageas 2014a). Vainshtein is also capable of screening large cosmological structures, while K-mouflage is not (Brax, Rizzo & Valageas 2015).

K-mouflage has been confronted with a number of cosmological data sets in Refs. Barreira et al. (2015b) and Benevento et al. (2019), with a review of current constraints given in Ref. Brax et al. (2021) and forecasts using spectroscopic and photometric primary probes by *Euclid* given in Ref. Frusciante et al. (2024). In particular, in Ref. Barreira et al. (2015b), the authors place a Solar System constraint on the coupling parameter $\beta_{\rm K} \leq 0.1$, and argue that the power-law form for $K(X)$ as chosen here will necessarily require a degree of fine tuning to avoid constraints. Despite this, this model is a good test case for implementation as it has been well studied in the literature and there are available N-body simulations with which to compare to (Hernández-Aguayo et al. 2022). More viable non-canonical kinetic terms can easily be implemented following the current implementations.

We alert the reader that we have made public a Mathematica notebook with some key Einstein frame quantities and derivations for the model along with this work. This contains useful expressions such as the exact solutions for the Einstein frame background $H(a)$ in the $n = 2$ and $n = 3$ cases.

2.3.2 Transformation to Jordan frame

In this section we provide some basic translations between Einstein and Jordan frames which will be useful for our comparisons of the K-mouflage model. We follow Ref. Francfort et al. (2019) for these expressions. We use subscripts 'J' and 'E' to denote Jordan and Einstein frame quantities, respectively.

The scale factor transforms as

$$a_{\rm J} = \bar{A}\, a_{\rm E}\,, \tag{16}$$

where $\bar{A}$ is the conformal factor evaluated at the background level (see equation 15). The Hubble rate transforms as

$$H_{\rm J}(a) = \frac{H_{\rm E}}{\bar{A}}\left[1 + \frac{\beta_{\rm K}}{M_{\rm pl}}\frac{{\rm d}\phi}{{\rm d}\ln a_{\rm E}}\right]\,. \tag{17}$$

The matter power spectrum transforms as (Francfort et al. 2019)

$$\begin{aligned}(2\pi)^3\delta_{\rm D}(\boldsymbol{k}_1+\boldsymbol{k}_2)P_{\rm J}(k_1) &= \langle\delta_{\rm J}(\boldsymbol{k}_1)\delta_{\rm J}(\boldsymbol{k}_2)\rangle \\ &= \langle\delta_{\rm E}(\boldsymbol{k}_1)\delta_{\rm E}(\boldsymbol{k}_2)\rangle \\ &- 4\frac{\bar{A}_\phi}{\bar{A}}\langle\delta_{\rm E}(\boldsymbol{k}_1)\delta\phi(\boldsymbol{k}_2)\rangle \\ &- 4\frac{\bar{A}_\phi}{\bar{A}}\langle\delta\phi(\boldsymbol{k}_1)\delta_{\rm E}(\boldsymbol{k}_2)\rangle \\ &+ 16\left(\frac{\bar{A}_\phi}{\bar{A}}\right)^2\langle\delta\phi(\boldsymbol{k}_1)\delta\phi(\boldsymbol{k}_2)\rangle\,,\end{aligned} \tag{18}$$

where and we used $\delta_{\rm J} = \delta_{\rm E} - 4\delta\phi\bar{A}_\phi/\bar{A}$, with $\bar{A}_\phi = {\rm d}\bar{A}(\phi)/{\rm d}\phi$, δ is shorthand for the matter density field perturbation $\delta_{\rm m}$, $\delta\phi$ is the scalar field perturbation, $\phi = \bar{\phi} + \delta\phi$, and k is the comoving Fourier mode in h Mpc^{-1}. Angular brackets denote an ensemble average. The linear order Klein–Gordon equation for the scalar field perturbation in Fourier space under the quasi-static approximation is (Brax & Valageas 2014b)

$$\delta\phi(\boldsymbol{k}) = -\frac{\bar{A}\beta_{\rm K}a^2}{M_{\rm pl}K_X k^2}\bar{\rho}_{\rm m}\delta_{\rm E}(\boldsymbol{k}), \tag{19}$$

where $K_X = {\rm d}\,K(X)/{\rm d}X$. Substituting $\delta\phi$ into equation (18) gives us the following relationship between linear matter power spectra predictions

$$P_{\rm L,J}(k) = P_{\rm L,E}(k)\left[1 + 2\mathcal{J}(k,a) + \mathcal{J}(k,a)^2\right]\,, \tag{20}$$

where

$$\mathcal{J}(k,a) = \frac{12\bar{A}_\phi\beta_{\rm K}H_0^2M_{\rm pl}\Omega_{\rm m,0}}{ak^2K_X}\,, \tag{21}$$

where we have used the relation $\bar{\rho}_{\rm m} = 3H_0^2M_{\rm pl}^2\Omega_{\rm m,0}a^{-3}$. We see that the linear matter power spectra in both frames are identical up to corrections that are suppressed by powers of $\sim H_0^2/k^2$.

It was argued in Ref. Francfort et al. (2019) that this correction to the matter power spectrum at non-linear scales continues to go as $\sim H^4/k^4$, and so becomes negligible on all sub-horizon scales. This argument hinged on a number of assumptions, including $A_\phi \sim$

[4]Not to be confused with the manifold $\mathcal{M}$ in equation (7).

$-A(\phi)/(2\phi)$. We will show in Section 4 that the corrections are indeed small at non-linear scales for the K-mouflage model, using the conformal factor given in equation (15).

3 TOOLS AND METHODS

In this section we give an overview of the methods developed to give predictions for the large-scale structure in all modified gravity scenarios considered. After explaining details of how we compute matter power spectra, we describe the methods we will compare in this work. Most of these are N-body simulation-based approaches with various degrees of approximation. The halo model reaction (Cataneo et al. 2019) is also considered, which is an analytic method based on the halo model and perturbation theory. Table 2 gives an overview of these methods.

3.1 $P(k)$ estimation

N-body simulations track the time-evolution of the matter distribution in the simulation box (of side $L_{\rm box}$) by means of a number of N-body particles ($N_{\rm P}$). To estimate the matter power spectrum from these sort of discrete distributions it is necessary to deal with some subtleties. The number of particles used in N-body simulations is often large (i.e. $10^8 - 10^{12}$) so that it would be computationally impractical to estimate the matter power spectrum by computing the distances between each pair of particles. Hence, the particles are normally interpolated on a regular grid using mass assignment schemes (MAS). Then the matter power spectrum is estimated exploiting the Fast Fourier Transform (FFT) algorithm. However, the modes close to the Nyquist frequency of the FFT grid can be significantly affected by aliasing (Jing 2005; Sefusatti et al. 2016). To avoid this problem we use the interlacing technique with the triangular-shaped-cloud MAS (Sefusatti et al. 2016) to compute the matter power spectra from the simulations. Aiming to compare our matter power spectra deep in the non-linear regime but mindful of the limited mass-resolution of our simulations, we use an FFT grid of size $N_{\rm mesh,1D} = L_{\rm box}/({\rm d}x)$ where ${\rm d}x$ is the domain grid resolution of the simulation, and use a simple linear binning with $k_{\rm min} = k_{\rm f}/2$ and $\Delta k = k_{\rm f}$, where $k_{\rm f} \equiv \frac{2\pi}{L_{\rm box}}$ is the fundamental frequency of the box.

3.2 Full-field solvers

Our reference predictions will come from numerical simulations that solve the non-linear Klein–Gordon equation, with multigrid relaxation, to get the precise modified force law. They also employ a large number of time-steps over which the particles are evolved, ensuring the accuracy of the resulting predictions. We consider two variants of these codes.

3.2.1 *ECOSMOG*

The `ecosmog` simulation code (Li et al. 2012; Li et al. 2013a) is a modified gravity extension of the adaptive mesh refinement (AMR) code RAMSES (Teyssier 2002). This code was used to simulate several gravity models in the literature:

(i) f(R) (Li et al. 2012);
(ii) nDGP (Li et al. 2013a);
(iii) symmetron (Davis et al. 2012; Brax et al. 2013);
(iv) dilaton (Brax et al. 2011);
(v) galileon (cubic, quartic, cubic vector) (Barreira et al. 2013a, b; Becker et al. 2020).

The accuracy of this code for predictions of $f(R)$ (Hu & Sawicki 2007) effects on the matter power spectrum has been estimated to be of ~ 1 per cent up to $k \sim 7\,h\,{\rm Mpc}^{-1}$ in the code comparison paper Ref. Winther et al. (2015). This code constitutes the highest precision predictive tool to be considered in this work.

3.2.2 *MG-GLAM*

`mg-glam` (Hernández-Aguayo et al. 2022; Ruan et al. 2022) extends the particle mesh (PM) code `glam` (Klypin & Prada 2018) to a general class of modified gravity theories (including the K-mouflage model) by adding extra modules for solving the Klein–Gordon equations, using the multigrid relaxation algorithm. It uses a regularly spaced 3D mesh covering the cubic simulation box, solves the Poisson equation for the Newtonian potential using the Fast Fourier Transform (FFT) algorithm, and adopts the Cloud-In-Cell (CIC) scheme to implement the matter density assignment and force interpolation.

`mg-glam` has been tested with the results from other high-precision modified gravity codes, such as `ecosmog` (Li et al. 2012, 2013a), `mg-gadget` (Puchwein et al. 2013), and `mg-arepo` (Arnold, Leo & Li 2019; Hernández-Aguayo et al. 2021). For example, using 1024^3 particles in a box of size $512\,{\rm Mpc}\,h^{-1}$, `mg-glam` simulations can accurately predict the matter power boost, $P_{\rm MG}/P_{\Lambda{\rm CDM}}$ at $k \lesssim 3\,h\,{\rm Mpc}^{-1}$, with about 1 per cent of the computational costs of the high-fidelity code `ecosmog`. Being the only code that has been used in the literature to simulate K-mouflage cosmologies, an estimate of its accuracy for the K-mouflage boost factor is not available. However it has been compared to the tree-PM code `mg-arepo` for another derivative coupling model (nDGP) where it showed an agreement of ~ 2 per cent up to $k = 3\,h\,{\rm Mpc}^{-1}$, with deviations of ~ 1 per cent from `mg-arepo` (and theory predictions) already present on linear scales.

3.3 Mg-evolution

We further consider the relativistic N-body code, `mg-evolution` (github; Hassani & Lombriser 2020). This code is based on `gevolution` (Adamek et al. 2016b), and integrates parametrized modifications of gravity. The parametrization framework includes both linear and deeply non-linear scales, with the non-linear parametrization being based on modified spherical collapse computations and a parametrized post-Friedmannian expression.

`mg-evolution` has been tested for a number of well-studied modified gravity models encompassing $f(R)$ and nDGP gravity that include large-field value and derivative screening effects (Hassani & Lombriser 2020). Unlike most modified gravity N-body implementations, `mg-evolution` is as fast as the ΛCDM simulations as it does not need to deal with solving computationally expensive scalar field equations.

In Section B we discuss the nDGP and CG implementations in `mg-evolution` through a parametrization with one screening transition, k_*, which is treated as a free parameter (see Section B). The effective gravitational constant is expressed as

$$\frac{\Delta G_{\rm eff}(k,a)}{G_{\rm N}} = \frac{\Delta G_{\rm eff,\,L}(a)}{G_{\rm N}} \times \frac{\Delta G_{\rm eff,\,NL}(k,a)}{G_{\rm N}}\,, \tag{22}$$

where we recall equation (5): $G_{\rm eff}(k,a) = G_{\rm N}[1 + \Delta G_{\rm eff}(k,a)/G_{\rm N}]$, $G_{\rm eff,\,L}$ denoting the linear regime parametrization

Table 2. Overview of the numerical codes employed in this comparison (for more information on screening approximations see the main text).

Code	Type	Screening approximation	Reference(s)
ecosmog	N-body (AMR)	Full K–G solution	Li et al. (2012)
mg-glam	N-body (uniform PM)	Full K–G solution	Hernández-Aguayo et al. (2022)
mg-evolution	N-body (uniform PM)	PPF with free parameter k_*	Adamek et al. (2016a, b); Hassani & Lombriser (2020)
hi-cola	N-body (PM in the 2LPT frame)	Screening factor	Wright et al. (2023), Gupta, Fiorini & Baker (2024)
cola-fml	N-body (PM in the 2LPT frame)	Linear K–G equation in Fourier space	Scoccimarro (2009); Winther et al. (2017); Brando et al. (2023)
react	Halo model and perturbation theory	Spherical collapse	Bose et al. (2023); Atayde et al. (2024)

Note: PPF: parametrized post-Friedmannian; PM: particle mesh; AMR: adaptive mesh refinement; 2LPT: 2nd order Lagrangian perturbation theory; K–G: Klein–Gordon.

and $G_{\rm eff,\,NL}$ refers to the parametrization of the non-linear regime that includes the screening or other suppression effects. The expressions for $G_{\rm eff,\,NL}$ are given in Section B. `mg-evolution` solves the modified Poisson equation (equation 4) based on $G_{\rm eff}$ obtained from equation (22). It is worth noting that this parametrization of gravitational modification is done in Fourier space. As detailed in Ref. Hassani & Lombriser (2020), this transformation yields an effective screening wavenumber k_*, which can be modelled (Lombriser 2016) for different screening types. Currently, as mentioned, we treat k_* as a free parameter to be set by the user. In this work we tune the values of k_* in order to optimize the agreement with the reference predictions in each model and at each redshift considered. The resulting values of k_* are presented in Section 4.

3.4 COmoving Lagrangian acceleration

The COmoving Lagrangian acceleration (COLA) method (Tassev et al. 2013) is a hybrid N-body approach to performing dark matter simulations to study the effects of gravity on the formation of large-scale structure. It leverages the fact that the growth of structure on large scales can be computed analytically through Lagrangian perturbation theory (LPT). This informs the small-scale N-body part of COLA codes, thereby allowing for a significant speedup in the production of results at the cost of a modest loss of accuracy at small scales. In short, the COLA approach is a method well-suited for producing large-scale structure results on mildly non-linear scales much faster than traditional N-body codes.

Since Tassev et al. (2013), implementations of COLA codes for modified gravity theories have followed for specific theories, such as f(R) and nDGP (Valogiannis & Bean 2017; Winther et al. 2017). Below we describe two branches of work that extend the COLA method to more general families of gravity models.

3.4.1 *Hi-cola*

Horndeski-in-COLA (`hi-cola`) (github; Wright et al. 2023) is an implementation of the COLA methodology for a subset of the Horndeski class (see equation 1). `hi-cola` aims not to carry hard-coded theory-specific implementations, but instead receives as input the Lagrangian functions for a given theory of interest, making it generic. The action of the new scalar degree of freedom, ϕ, is included as a fifth force in the COLA simulation.

After receiving inputs for the forms of the Horndeski functions, G_2, G_3, and G_4, the symbolic manipulation modules of `hi-cola` construct the appropriate background equations of motion and background-dependent fifth force expressions and solves them. These are used to handle the expansion of the simulation box, compute second-order LPT factors (2LPT) and construct the total force experienced by dark matter particles. This force can be schematically written as

$$F_{\rm total} = G_{\rm eff}\, F_{\rm N}, \tag{23}$$

where

$$G_{\rm eff} = \frac{G_{\rm G4}}{G_{\rm N}}\left\{1 + \beta_{\rm HC}(z) S_{\rm HC}(z, \delta_m)\right\}. \tag{24}$$

$F_{\rm N}$ is the regular Newtonian force which is present in GR, and the multiplicative factor in braces represents the extra force contributions from ϕ. $G_{\rm G4}$ is the effective gravitational constant, which can differ from $G_{\rm N}$ in a time-dependent manner if G_4 in equation (1) is non-trivial. This term will play a role in the results of Section 4.2.3.

$\beta_{\rm HC}$ is a background-dependent function known as the *coupling factor*; it controls the total possible strength of the fifth force at a given point in time. $S_{\rm HC}$ is a background and density-dependent function called the *screening factor*. On linear scales $S_{\rm HC} \to 1$, whilst in screened regimes $S_{\rm HC} \to 0$. Hence this factor is responsible for the suppression of the fifth force in on small scales, returning the theory's behaviour to GR.

$S_{\rm HC}$ is derived under a quasi-linear perturbative treatment, where the metric perturbations are considered to first order, whilst the scalar field *derivative* perturbations are kept up to third order, following Ref. Kimura, Kobayashi & Yamamoto (2012). Combined with the assumptions that the quasi-static approximation holds and that the matter overdensity is distributed spherically in space leads to the analytic form of $S_{\rm HC}$ (see equation 3.15 in Wright et al. 2023). These assumptions in the derivation of $S_{\rm HC}$ lead to a caveat: that in its current public state, `hi-cola` is designed to work with theories that exhibit *Vainshtein* screening. However, recent development of `hi-cola` has focused on extending the formalism to other screening mechanisms like K-mouflage, and these results are presented in Section 4.2.3. The full details of K-mouflage in `hi-cola` are provided in Ref. Gupta et al. (2024).

3.4.2 *COLA-FML*

In this subsection we describe another approximate simulation method to modified gravity theories endowed with the Vainshtein mechanism, such as nDGP and the Galileon theory family. This method was initially proposed in Ref. Scoccimarro (2009), and later revisited in Ref. Brando et al. (2023). It consists of linearizing the Klein–Gordon equation in Fourier space, and implementing a resummation scheme to find a function, $G_{\rm eff}(k, a)$, defined in the same way as equation (22), that approximately captures the non-linear corrections introduced by the Vainshtein mechanism on small scales. Specifically, this function transitions between an unscreened regime at large scales, where $G_{\rm eff}(k, a) \to G_{\rm eff,L}(a)$, to the small scale regime where GR is recovered, $G_{\rm eff}(k, a) \to G_{\rm N}$.

In order to do so, in Refs. Scoccimarro (2009) and Brando et al. (2023) the authors require the non-linear function,

$\Delta G_{\rm eff,\,NL}(k,a)/G_{\rm N}$,[5] has the screening property, i.e.

$$\frac{\Delta G_{\rm eff,\,NL}(k,a)}{G_{\rm N}}\,(k/k_* \ll 1) \to 1,$$
$$\frac{\Delta G_{\rm eff,\,NL}(k,a)}{G_{\rm N}}\,(k/k_* \gg 1) \to 0\,, \tag{25}$$

where k_* is the wavenumber associated with the Vainshtein radius, defined in equation (B3). The specifics behind the computation of the function $\Delta G_{\rm eff,\,NL}(k,a)/G_{\rm N}$ is explicitly shown in Ref. Brando et al. (2023). This screening approximation scheme has the advantage of not introducing additional screening parameters used to tune the approximate results with results from N-body simulations that consistently solve the full Klein–Gordon equation at each time-step of the simulation. The whole dependence of the gravity theory is encoded in the $\Delta G_{\rm eff,\,NL}(k,a)/G_{\rm N}$ function.

The methodology of this approximate method for Vainshtein screening is computed using an external `python` notebook, where one can follow the steps outlined in Ref. Brando et al. (2023) to compute $G_{\rm eff}(k,a)$ externally. With the tabulated function computed, the results are then implemented in the `cola-fml` (github) N-body solver, that implements the COLA method in a parallelized manner, ideal for fast and approximate simulations. The `cola-fml` library also has different screening approximations for theories other than the ones considered here, and are presented in Ref. Winther & Ferreira (2015a). Importantly for this paper, our results for the $G_{\rm eff}(k,a)$ screening case will be different than the ones of `hi-cola` at non-linear scales, however, at linear scales the two codes are identical.

3.5 Halo model reaction

The halo model reaction (Cataneo et al. 2019) is a flexible, accurate, and fast means to model the non-linear matter power spectrum in beyond-ΛCDM scenarios. This model has been demonstrated to align with N-body simulations at the 2 per cent level down to $k = 3\ h\,{\rm Mpc}^{-1}$, with minor variations depending on redshift, the extent of modification to GR, and the mass of neutrinos (Cataneo et al. 2020; Bose et al. 2021). The method aims to model non-linear corrections to the matter power spectrum resulting from modified gravity through a reaction function $\mathcal{R}(k,z)$, which incorporates both 1-loop perturbation theory and the halo model (see Bernardeau et al. 2002; Cooray & Sheth 2002, for reviews). In this framework, the non-linear matter power spectrum is expressed as the product

$$P_{\rm NL}(k,z) = \mathcal{R}(k,z)\,P_{\rm NL}^{\rm pseudo}(k,z)\,, \tag{26}$$

where the pseudo power spectrum is defined such that all non-linear physics are modelled using GR but the initial conditions are adjusted to mimic the modified linear clustering at the target redshift.

The halo model reaction without massive neutrinos, $\mathcal{R}(k,z)$, is given as a corrected ratio of target-to-pseudo halo model spectra

$$\mathcal{R}(k,z) = \frac{\{[1-\mathcal{E}(z)]\,e^{-k/k_\star(z)} + \mathcal{E}(z)\}\,P_{\rm 2H}(k,z) + P_{\rm 1H}(k,z)}{P_{\rm hm}^{\rm pseudo}(k,z)}\,. \tag{27}$$

The components are explicitly given as

$$P_{\rm hm}^{\rm pseudo}(k,z) = P_{\rm 2H}(k,z) + P_{\rm 1H}^{\rm pseudo}(k,z), \tag{28}$$

$$\mathcal{E}(z) = \lim_{k\to 0}\frac{P_{\rm 1H}(k,z)}{P_{\rm 1H}^{\rm pseudo}(k,z)}, \tag{29}$$

$$k_\star(z) = -\bar{k}\left\{\ln\left[\frac{A(\bar{k},z)}{P_{\rm 2H}(\bar{k},z)} - \mathcal{E}(z)\right] - \ln\left[1-\mathcal{E}(z)\right]\right\}^{-1}, \tag{30}$$

[5]We note that in Ref. Brando et al. (2023) this function is called $M(k,a)$.

with

$$A(k,z) = \frac{P_{\rm 1-loop}(k,z) + P_{\rm 1H}(k,z)}{P_{\rm 1-loop}^{\rm pseudo}(k,z) + P_{\rm 1H}^{\rm pseudo}(k,z)}\,P_{\rm hm}^{\rm pseudo}(k,z) - P_{\rm 1H}(k,z)\,. \tag{31}$$

$P_{\rm 2H}(k,z)$ is the 2-halo term which we approximate with the linear matter power spectrum, $P_{\rm L}(k,z)$. $P_{\rm 1H}(k,z)$, and $P_{\rm 1H}^{\rm pseudo}(k,z)$ are the 1-halo terms as predicted by the halo model, with and without modifications to the standard spherical collapse equations, respectively. Recall that by definition, the pseudo cosmology has no non-linear beyond-ΛCDM modifications. Similarly, $P_{\rm 1-loop}(k,z)$ and $P_{\rm 1-loop}^{\rm pseudo}(k,z)$ are the standard perturbation theory 1-loop matter power spectra with and without non-linear modifications to ΛCDM, respectively. As in the literature, equation (29)'s limit is taken to be at $k = 0.01\ h\,{\rm Mpc}^{-1}$ and $k_\star$ is computed using $\bar{k} = 0.06\ h\,{\rm Mpc}^{-1}$.

The nDGP model was part of the initial release of the publicly available halo model reaction code, `React` (Bose et al. 2020). This code has been updated to include massive neutrinos in Ref. Bose et al. (2021) and model-independent parametrizations in Ref. Bose et al. (2023), which constituted version 2 of the code (github). The GCCG model was recently implemented in this version of `react` (Atayde et al. 2024), which is employed in Section 4 in the CG limit. The K-mouflage patch is being made public with this work and we give all the relevant expressions in Section A.

For the pseudo spectrum appearing in equation (26) we use `hmcode2020` (Mead et al. 2021). This is currently the most accurate and flexible prescription for the pseudospectrum and has been tested in a number of works (see for example Cataneo et al. 2019; Bose et al. 2021, 2023). It is more accurate than the halofit prescription of Ref. Takahashi et al. (2012), quoting a $2.5-5$ per cent accuracy for $k \leq 1\ h\,{\rm Mpc}^{-1}$. It can also accommodate modifications that induce an additional scale dependence in the linear matter power spectrum. For modifications that only introduce a scale-independent shift in the linear spectrum amplitude, more accurate emulators can be used, such as the `euclidemulator2` (Knabenhans et al. 2019), which are quoted to be 1 per cent accurate when compared to high fidelity N-body simulations down to $k \leq 10\ h\,{\rm Mpc}^{-1}$. Despite this, the reaction function $R(k,z)$ is only expected to be 1 per cent accurate for $k \leq 1\ h\,{\rm Mpc}^{-1}$ (Cataneo et al. 2019).

It is also worth noting that `euclidemulator2`'s internal accuracy is restricted to a hyperspheroidal region of their parameter space. Points outside this region might have considerable degradation in accuracy. This is considerably important in the context of beyond-ΛCDM scenarios as we need tools that work in extreme regions of the parameter space. For these reasons, work is currently being undertaken to build a pseudospectrum emulator based on appropriate numerical simulations (Giblin et al. 2019).

The choice of `hmcode2020` keeps in line with the halo model reaction's claim of generality, while maintaining competitive accuracy within the reaction's per cent-level accuracy range, especially when taking the ratio of modified to unmodified spectra, i.e. the matter power spectrum boost (see equation 32).

4 RESULTS

Our main results are the comparisons of the non-linear matter power spectrum between the different codes. Specifically, we consider the models described in Table 3 for which we have N-body simulations that solve the full scalar field equation of motion available to use as benchmarks. We list the specifications of each simulation ran for these comparisons below. These include: box size ($L_{\rm box}$), number

Table 3. Models considered in this work. The ΛCDM $\sigma_8(z=0) = 0.851, 0.805, 0.815$ for nDGP, CG, and K-mouflage cosmologies, respectively. We remind the reader that the values for $\{s, q\}$ are fixed in CG, while adopting the tracker solution for the scalar field imposes the values for c_2 and c_3 quoted in the table.

Parameter	nDGP-N1	nDGP-N5	CG	QCDM	K-mouflage – A	K-mouflage – B	K-mouflage – C
$\Omega_{m,0}$	0.281		0.313			0.3089	
$\Omega_{b,0}$	0.046		0.049			0.0486	
H_0	69.7		67.32			67.74	
n_s	0.971		0.9655			0.9667	
A_s	2.297×10^{-9}		2.010×10^{-9}			2.064×10^{-9}	
$\sigma_8(z=0)$	0.912	0.865	0.884	0.865	0.881	0.852	0.837
Ω_{rc}	0.25	0.01	–	–	–	–	–
$c_2/c_3^{2/3}$	–	–	−5.378	–	–	–	–
c_3	–	–	10	–	–	–	–
s	–	–	2.0	–	–	–	–
q	–	–	0.5	–	–	–	–
n	–	–	–	–	2	2	2
λ	–	–	–	–	1.475	1.460	1.452
K_0	–	–	–	–	1	10	1
β_K	–	–	–	–	0.2	0.2	0.1

of particles (N_P), particle mass (m_P), grid cells (N_g), initial redshift (z_{ini}), and force resolution.

(i) `ecosmog` runs: $L_{box} = 1024$ Mpc h^{-1}, $N_P = 1024^3$, $m_P \simeq 7.8 \times 10^{10}\ M_\odot\, h^{-1}$. The initial conditions are generated at $z_{ini} = 49$ by `mpgrafic` (Prunet et al. 2008) using the Zel'dovich approximation. It uses a force resolution of ~ 15.6 kpc h^{-1}.

(ii) `mg-glam` runs: $L_{box} = 512$ Mpc h^{-1}, $N_P = 1024^3$, $N_g = 2048^3$, $m_P = 1.07 \times 10^{10}\ M_\odot\, h^{-1}$, where N_g is the number of grid cells. Initial conditions are generated at $z_{ini} = 100$ using `glam`'s own initial condition generator. It uses a fixed force resolution of 250 kpc h^{-1} with an adaptive time-stepping described in the original `glam` paper (Klypin & Prada 2018).

(iii) `mg-evolution` runs: The nDGP simulation runs use $L_{box} = 1000$ Mpc h^{-1} with $N_g = N_p = 1024^3$. The initial conditions are generated at $z_{ini} = 49$. For the CG case, the initial conditions are the same as in the `cola` runs. These runs use $L_{box} = 400$ Mpc h^{-1}, $N_P = N_g = 512^3$.

(iv) `cola` runs: $L_{box} = 400$ Mpc h^{-1} and $N_P = 512^3$ with initial conditions generated using 2LPT for all simulations. For K-mouflage: $m_P \simeq 4.1 \times 10^{10}\ M_\odot\, h^{-1}$. Initial conditions are generated at $z_{ini} = 19$. For nDGP: $m_P \simeq 3.7 \times 10^{10}\ M_\odot\, h^{-1}$. Initial conditions are generated at $z_{ini} = 49$. For CG and QCDM: $m_P \simeq 4.1 \times 10^{10}\ M_\odot\, h^{-1}$. Initial conditions are generated at $z_{ini} = 49$.

Before presenting the spectra comparisons, we take a look at how each model presented in Section 2 modifies the standard ΛCDM background evolution. This background evolution is adopted for each of the different codes and so differences seen in the following section only arise from how the perturbations are treated.

4.1 Background evolution

In Fig. 1 we show the modification to the standard ΛCDM background expansion for the models described in Table 3. We remind the reader that we assume a ΛCDM expansion for the nDGP models and so this is not shown. We see that the QCDM and CG cases give a much larger modification at late times than any of the K-mouflage models in the Einstein frame. In all models, we see a slower expansion rate at roughly $a > 0.2$ which acts to enhance structure formation. Indeed, the σ_8 is larger for the QCDM model than for both K-mouflage models B and C (see Table 3), despite having a lower A_s (although the QCDM cosmology has a slightly larger $\Omega_{m,0}$). In all cases, the maximum modification is ~ 8 per cent (QCDM), with the K-mouflage models giving a maximum modification of 3 per cent at $a = 0.5$.

In the same figure we also show the modification in the Jordan frame for the K-mouflage models (middle panel). We see here that relative to ΛCDM, we have a significantly slower expansion at $a > 0.03$, with a maximum modification of 11 per cent at $a \sim 0.4$. Further, the current day expansion is larger than the one expected from ΛCDM by 5 per cent under the strongest modification considered here. We do remind the reader that the free parameter λ has been tuned to match the current day expansion rate in ΛCDM in the Einstein frame. These panels show that relatively large differences can be observed at the background level when switching frames, which we will see in the next subsection are not evident at the level of the perturbations (also see Section 2.3.2).

4.2 Matter power spectrum boost

Next we take a look at the perturbations, specifically how the matter power spectrum is modified over ΛCDM. For this, we consider the modified gravity boost, defined as

$$B(k,z) \equiv \frac{P_{NL}(k,z)}{P_{NL}^{\Lambda CDM}(k,z)}\,. \tag{32}$$

4.2.1 nDGP

In Fig. 2 we show how the various predictions for the boost compare, using the `ecosmog` measurements as a reference, for the nDGP cosmologies found in Table 3. Boost comparisons for nDGP amongst different codes have already been performed extensively in the literature, and so this case is shown mainly as a consistency check, but also to compare the `hi-cola` implementation which has not yet been tested before.

We find that for the low modification case, N5, all predictions remain within 1 per cent of each other for $k \leq 3\ h$ Mpc^{-1}, including the linear prediction, which at $z = 0$ gives a modification of $B(k \to 0, z = 0) = 1.033$. For N1, $B(k \to 0, z = 0) = 1.149$ per cent. In this case, all predictions except the linear remain within 2 per cent

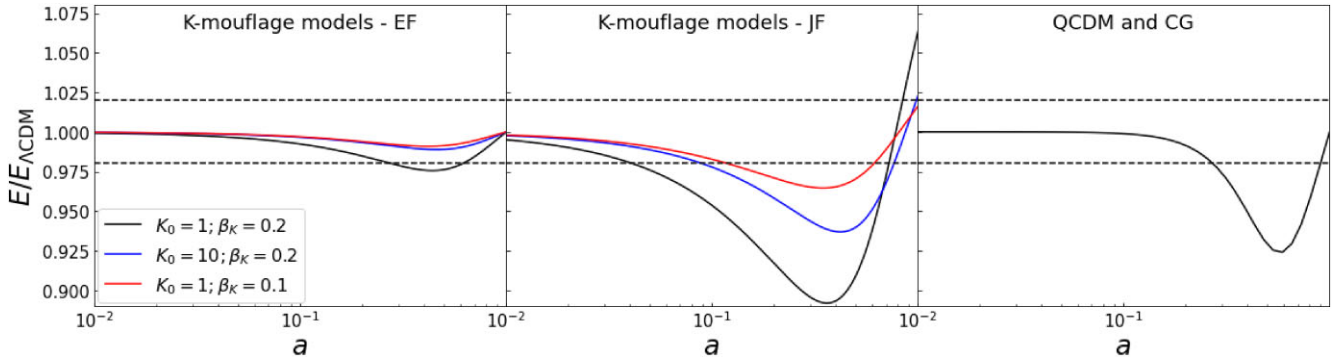

Figure 1. The ratio of the normalized Hubble expansion rate ($E(a) = H(a)h_0^{-1}$) between the modified gravity and GR models. The left panel shows the K-mouflage models shown in Table 3 in the Einstein frame, while the middle panel shows the same models in the Jordan frame, with a now being the Jordan frame scale factor. The right panel shows the QCDM model, which has the same background expansion as the CG model. The model parameters for K-mouflage are defined in Section 2.3.

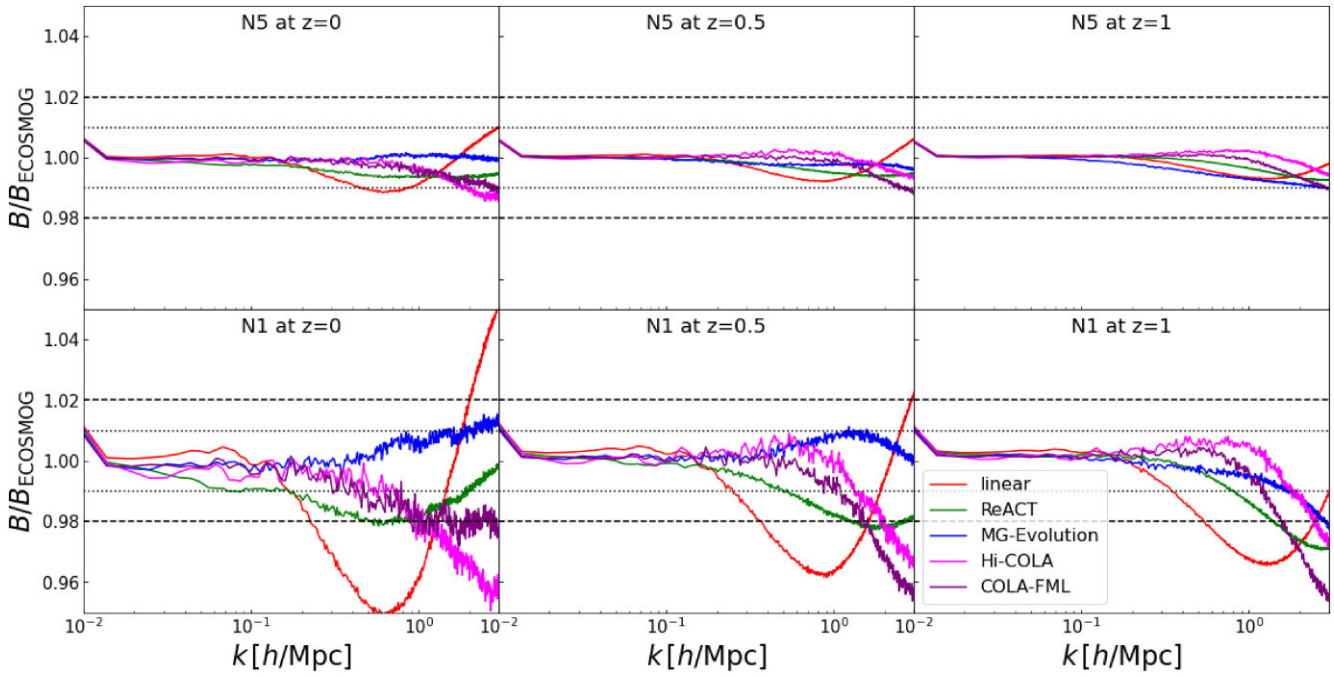

Figure 2. Comparing boost factors for the various codes listed in Table 2 for nDGP at $z = 0, 0.5, 1$ (from left to right) with `ecosmog` as benchmark. The upper panels show the results for the nDGP-N5 (low modification) model and the lower panels for the nDGP-N1 (high modification) model (see Table 3).

of the `ecosmog` reference for $k \leq 1\ h\,\mathrm{Mpc}^{-1}$. `mg-evolution` performs the best as expected, having an additional free parameter giving the screening transition, k_*. We have found $k_* = 2\ h\,\mathrm{Mpc}^{-1}$ and $k_* = 1\ h\,\mathrm{Mpc}^{-1}$ give a good overall agreement with the `ecosmog` simulations for the N1 and N5 models respectively. Using these values the `mg-evolution` boost remains within 1 per cent up to $k \leq 3\ h\,\mathrm{Mpc}^{-1}$ except for the largest modes at $z = 1$ where it worsens to 2 per cent, consistent with what was found in Ref. Hassani & Lombriser (2020). Similarly, the halo model reaction remains within 2 per cent for $k \leq 3\ h\,\mathrm{Mpc}^{-1}$ except for the largest modes at $z = 1$, where it worsens to 3 per cent agreement, in accordance with Ref. Cataneo et al. (2019).

The two COLA methods show similar agreement, but deviate the most on average from the reference boost measurements. `cola-fml` performs slightly better at $z = 0$ while `hi-cola` does better at higher z, with deviations up to 4 per cent at $k = 3\ h\,\mathrm{Mpc}^{-1}$. This is very consistent with the results of Ref. Winther et al. (2017).

4.2.2 *Cubic Galileon (CG)*

Fig. 3 shows the boost comparisons between the various codes for the CG and QCDM cases, again using `ecosmog` as a reference. These `ecosmog` simulations were ran using the same code as presented in Ref. Barreira et al. (2013a). We have changed the baseline cosmology for these new runs, particularly lowering the value of A_s and H_0. We also run a ΛCDM counterpart with which to calculate equation (32). Previous works have compared the boost ratio of the CG spectrum to that in QCDM (Wright et al. 2023), or have performed direct spectra comparisons (Atayde et al. 2024). Further, in Ref. Atayde et al. (2024) the authors found significant disagreement when using an `hmcode2020` prescription, which was outperformed by the halofit pseudospectrum prescription. This was being caused by the σ_8-dependent damping introduced into `hmcode2020` (Mead et al. 2021), which was not calibrated for particularly high values of σ_8 as that of the simulations found in Ref. Barreira et al. (2013a). The

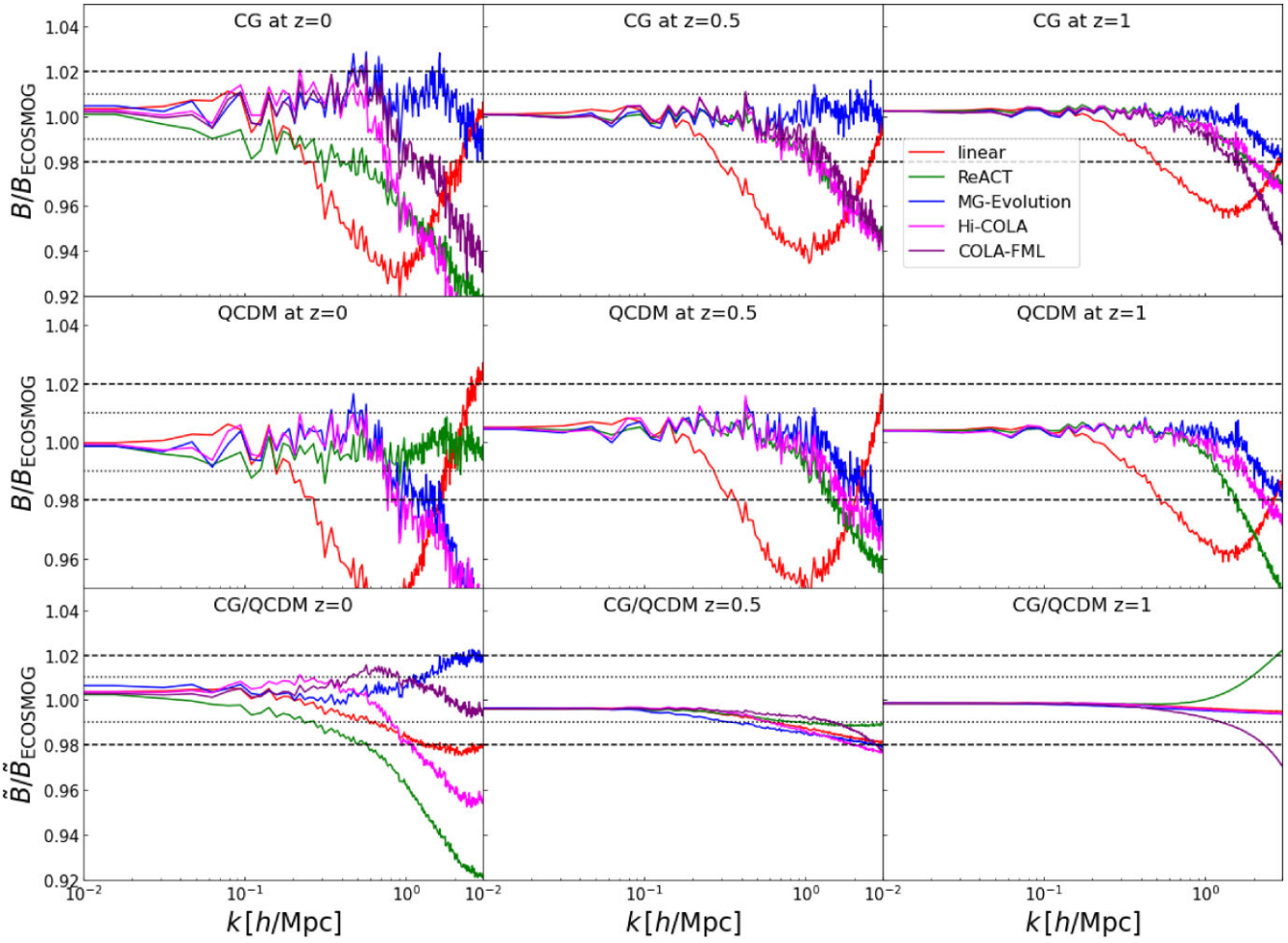

Figure 3. Comparing boost factors for the various codes listed in Table 2 for the CG (upper) and QCDM (middle) and QCDM-based boost (bottom) at $z = 0, 0.5, 1$ (from left to right) with `ecosmog` as the benchmark. Note `cola-fml` and `hi-cola`'s results for QCDM are identical and so we only show the Hi-cola QCDM ratio in the middle panels.

lower value of σ_8 in our simulations was found to greatly improve the performance of `hmcode2020` over halofit. For comparison with previous work, we also show the comparisons for the ratio of CG to QCDM power spectra, or QCDM-based boost, in the bottom panels of Fig. 3.

The `mg-evolution` predictions again give the best agreement, remaining within 1 per cent in the CG case at $z \geq 0.5$ down to $k = 3\,h\,\mathrm{Mpc}^{-1}$. At $z = 1$, the linear implementation, or equivalently $k_* \to \infty$, provides the best match. However, in the figure, we have plotted the case $k_*(z \geq 0.5) = 6\ h\,\mathrm{Mpc}^{-1}$ as it appears to work well given the resolution of the simulation. Adopting the value $k_* = 6\,h\,\mathrm{Mpc}^{-1}$ at $z = 0$ causes a quick divergence of the predictions, with an 8 per cent disagreement at $k = 1\ h\,\mathrm{Mpc}^{-1}$. This is expected as k_* controls the screening Fourier mode, which will be smaller at low redshift when densities are larger. Adopting $k_* = 0.4\ h\,\mathrm{Mpc}^{-1}$ at $z = 0$ brings the predictions to within 2 per cent agreement in the same range of scales.

Interestingly, in the QCDM-based boost case we can adopt the same value of $k_* = 0.3\ h\,\mathrm{Mpc}^{-1}$ for all redshifts considered while keeping a good fit to the `ecosmog` measurements. In this case, the predictions are consistent within 1 per cent down to $k = 1\ h\,\mathrm{Mpc}^{-1}$. The disagreement for $k > 1\ h\,\mathrm{Mpc}^{-1}$ arises from resolution effects, as supported by the agreement between `mg-evolution` and `hi-cola`, which both have the same resolution. This suggests that the tuning of k_* performed to match the reference boost factor in the CG case is partially compensating for the resolution-induced loss of boost.

The halo model reaction remains within 1 per cent for $k \leq 1\ h\,\mathrm{Mpc}^{-1}$ for both QCDM and CG cases, with the exception of the CG case at $z = 0$. Here we find up to 4 per cent disagreement with `ecosmog`. This is an atypically large disagreement given the similarity of CG to nDGP, for which the halo model reaction performs significantly better. To investigate this, we have tested different pseudo spectra prescriptions, specifically halofit and `euclidemulator2`, neither offering significant improvement for the matter power spectrum boost. We have also tried omitting the 1-loop correction (see equation 31) with little change to the predictions as found in Ref. Bose et al. (2023). The excellent agreement in the QCDM case (middle panels) at $z = 0$, with 1 per cent agreement beyond $k = 3\ h\,\mathrm{Mpc}^{-1}$, indicates no issue in the background implementation. We have also checked the QCDM-based boost (bottom panels), where the denominator in equation (32) is now QCDM instead of ΛCDM. These comparisons show the same disagreement at $z = 0$ as in the CG ΛCDM-based boost case, but the same or better agreement at higher redshifts. The improved agreement at $z \geq 0.5$ in the QCDM-based boost case is just a partial

cancellation of inaccuracies in the QCDM and CG ΛCDM-based boost cases.

Lastly, we also checked the behaviour of the reaction function $\mathcal{R}$ for varying GCCG modification strengths by changing the value of s. We compared these to corresponding nDGP predictions for $\mathcal{R}$ such that the nDGP models gave the same linear enhancement of structure as the GCCG cases, making their pseudo spectra identical. We observed significantly more suppression coming from $\mathcal{R}$ in the GCCG than nDGP, especially for large modifications (large s or large $\Omega_{\rm rc}$). This added suppression of power may be due to the G_2 term present in the GCCG. We do note that the CG has a very large linear enhancement of clustering at $z = 0$, equivalent to a nDGP model with $\Omega_{\rm rc} = 0.6$. This may indicate a break down of the halo model reaction's assumptions, specifically the ΛCDM fits it assumes for the halo mass function and virial concentration. The latter has been shown to significantly impact its accuracy (Cataneo et al. 2019; Srinivasan et al. 2021; Srinivasan, Thomas & Battye 2024), especially when the modification to gravity is large. To further pin the $z = 0$ CG disagreement down, we would need to run a CG pseudo cosmology simulation which would make it clear whether or not the reaction function modelling or ΛCDM-fits in the halo model components are failing. GCCG simulations with a smaller modification will also help illuminate the accuracy of the current reaction function implementation. This will be the focus of future work.

Finally, both COLA implementations remain 2 per cent consistent with `ecosmog` in the CG case at scales $k \leq 1\ h\,\mathrm{Mpc}^{-1}$. `cola-fml` performs slightly better at low z while `hi-cola` shows better agreement at higher z. The implementations differ only in their approach to screening and so we only show the `hi-cola` results for QCDM, where it is similarly consistent to `ecosmog` as in the CG case. We note that all codes tend to underpredict the boost at small scales. Part of this difference surely comes from the fact that while the `ecosmog` code consistently solves the full Klein–Gordon equation, the other codes implement the screening mechanism in an approximate way, making use of the spherical approximation in one way or another. Therefore, at smaller scales these approximate methods are not guaranteed to be valid. A better test of the accuracy of screening is provided by the QCDM-based boost in the bottom panels, where we see far better agreement between the COLA methods and `ecosmog`.

On this note, we remark that both COLA and `mg-evolution`'s disagreement with the benchmarks in both nDGP, CG, and QCDM cases is also partially due to a low force resolution which can lead to a loss of power on small scales (see Brando et al. 2022, for example). By increasing the force resolution, and time-steps in the COLA cases, we expect to find much better agreement above $k = 1\ h\,\mathrm{Mpc}^{-1}$, particularly in the QCDM case which does not have screening. We note that the limited force accuracy will affect all particle mesh codes, including `mg-glam`, and the most efficient and sure way to go to smaller scales would be to use Tree-particle mesh or AMR codes like `ecosmog`.

4.2.3 *K-mouflage*

For K-mouflage, we restrict our comparisons to `mg-glam`, `hi-cola`, and `react` with the `mg-evolution` implementation to be the focus of an upcoming work. We expect the same level of accuracy as exhibited in the CG and nDGP cases, especially given the freedom imparted by k_*.

In Fig. 4 we show the results for the K-mouflage model. As a reference we use the `mg-glam` simulations, ran for the purpose of this comparison. We compare the K-mouflage boost for the three models listed in Table 3, all of which assume $n = 2$ in equation (14). We begin by noting that the coupling of matter to the scalar field is proportional to $\beta_{\rm K}/K_0$ (see equation 81 of Brax & Valageas 2014b, for example), and so large positive K_0 decreases the fifth force while large $\beta_{\rm K}$ increases it. We find the larger the modification, the worse the agreement between `react`, `hi-cola`, and `mg-glam`. We can see this by moving from top to bottom panels in Fig. 4. Further, we note for the largest modification (top panels), there is a 1 per cent offset between `mg-glam` and linear theory (as well as the other codes). This was also seen in fig. 10 of Ref. Hernández-Aguayo et al. (2022) but not seen in the linearized simulations presented in that reference, suggesting this is a consequence of the non-linear treatment of `mg-glam`. We also note much smaller linear theory offsets at large scales for the weaker modifications.

For the strongest modification, K-mouflage A in Table 3, at low z, all codes are consistent within 2 per cent for $k \leq 1\ h\,\mathrm{Mpc}^{-1}$. This agreement improves for the halo model reaction to 1 per cent agreement for $k \leq 3\ h\,\mathrm{Mpc}^{-1}$ at $z = 1$ and in the weakest modification case, K-mouflage C (see Table 3). Overall, `hi-cola` does not show significant improvement or degradation with redshift or modification strength, consistently remaining within 2 per cent for $k \leq 3\ h\,\mathrm{Mpc}^{-1}$. The exception is K-mouflage A at $z = 0$ (upper left panel), where it degrades to 4 per cent discrepancy at $k = 3\ h\,\mathrm{Mpc}^{-1}$. The `hi-cola` predictions are all made in the Jordan frame while `mg-glam` and `react` produce predictions in the Einstein frame. It is here we note the consistency of the non-linear matter power spectrum in both frames, supporting the claim of Ref. Francfort et al. (2019).

Before concluding we make some technical notes on the comparisons. In the case of the Jordan frame predictions from `hi-cola`, the boost is taken with the K-mouflage spectrum measured at $a_{\rm J}$, calculated using equation (16). The inclusion of K-mouflage theories in `hi-cola` was presented in Ref. Gupta et al. (2024). Finally, we note that `react` has the option to use the PPF screening formalism for K-mouflage as derived in Ref. Lombriser (2016), and which we present in Section B for completeness. This framework comes with an additional degree of freedom and so we have chosen not to use this in our comparisons.

5 CONCLUSIONS

High quality N-body codes for modified gravity are essential in order to place reliable constraints on gravity using LSS observations. Ongoing galaxy surveys such as *Euclid* or the Dark Energy Survey will heighten their necessity by beating down the statistical uncertainty on our measurements, making theoretical accuracy essential. Benchmarking the accuracy of approximate but computationally efficient numerical methods against these high-quality simulations is an important step towards reliable constraints from the forthcoming data.

In this paper we have performed comparisons of the matter power spectrum modification induced by three distinct theories of modified gravity, each of which induces a scale-independent enhancement of the linear growth of structure: the normal branch of the DGP braneworld model, the Cubic Galileon, and K-mouflage. The former two employ the Vainshtein screening mechanism, while the latter employs the K-mouflage screening mechanism. For similar comparisons with scale-dependent modifications to the linear growth and the chameleon (Khoury & Weltman 2004) or symmmetron (Hinterbichler & Khoury 2010) screening mechanisms, we refer the reader to Refs. Winther et al. (2015, 2017), Cataneo et al. (2019), Hassani & Lombriser (2020), and Adamek et al. (2024).

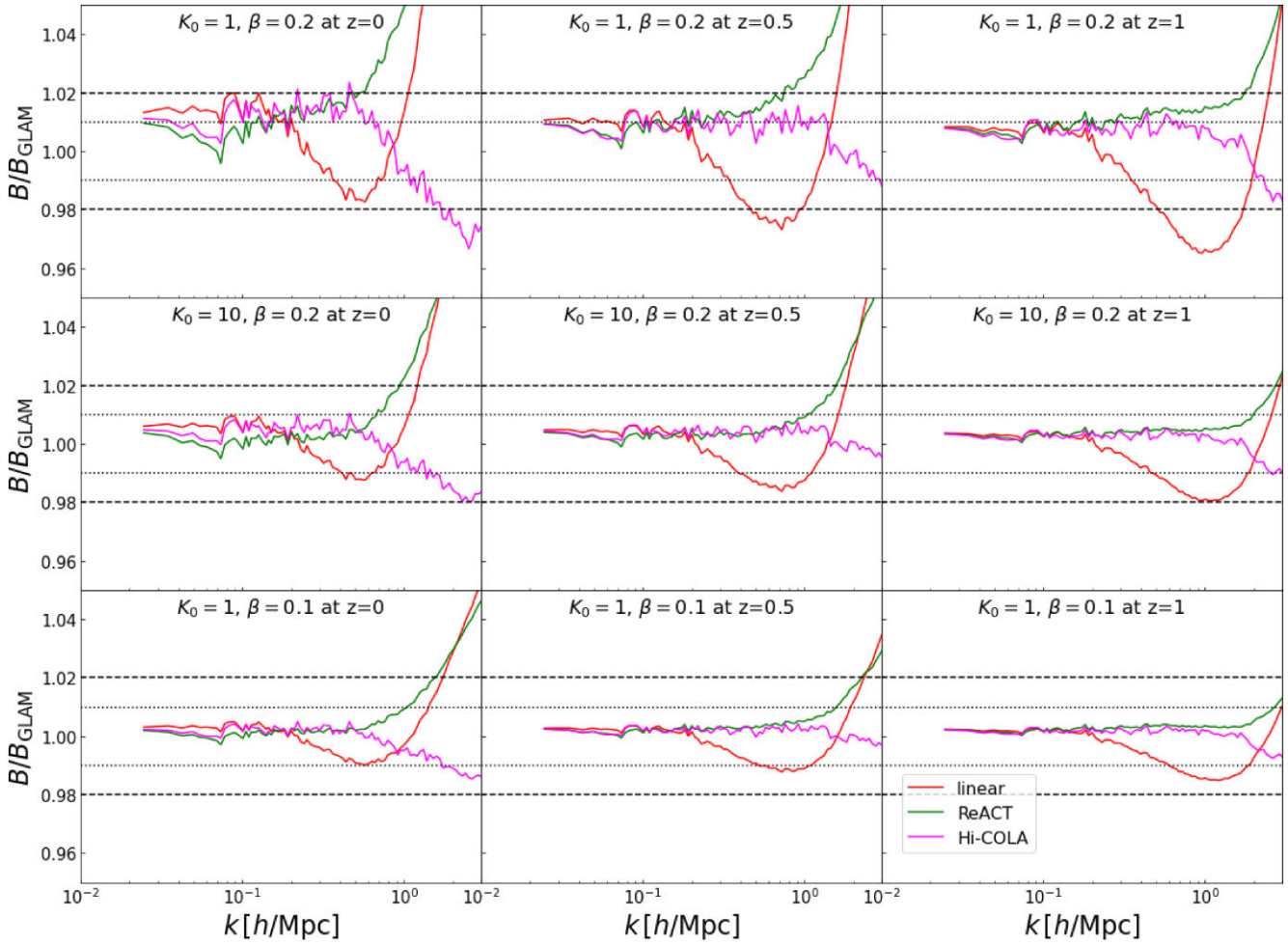

Figure 4. Comparing boost factors for the various codes listed in Table 2 for the K-mouflage models listed in Table 3 with $\{K_0, \beta_K\} = \{1, 0.2\}, \{10, 0.2\}, \{1, 0.1\}$ (from top to bottom) at $z = 0, 0.5, 1$ (from left to right) with `mg-glam` as the benchmark. All models assume $n = 2$.

We compare the matter power spectrum boost predicted by six different numerical codes, each of which has a varying approach to the non-linear gravitational coupling: full-field solvers (`ecosmog` and `mg-glam`), COLA of which we compare two distinct codes, `hi-cola` and `cola-fml`, the relativistic parametrized N-body code, `mg-evolution`, and the semi-analytic halo model reaction approach expressed by the `react` code. We summarize the distinctions of each code below:

(i) **ecosmog & mg-glam**: Solve the Klein–Gordon equation exactly to get the force applied to particles in a box. Serve as accuracy benchmarks.

(ii) **hi-cola**: Includes a fifth force in the COLA formalism via a screening factor, as well as consistently solving the modified cosmological expansion history. Screening factors are derived using a quasi-linear treatment of the metric and scalar field perturbations, along with assuming the quasi-static approximation and spherically distributed overdensities.

(iii) **cola-fml**: Introduces the Vainshtein mechanism by evaluating a function, $G_{\rm eff}(k, a)$, that captures on average non-linear corrections from the screening mechanism. This method is performed by linearizing the Klein–Gordon equation in Fourier space, and the full function is found by an iterative process.

(iv) **mg-evolution**: Employs a parametrized ansatz for the non-linear force law which comes with a screening parameter.

(v) **react**: Uses spherical collapse, the halo model, and 1-loop perturbation theory to predict the matter power spectrum.

We summarize the overall accuracy exhibited by each approach in Table 4 with respect to the full-field-solver benchmark. We remark that N-body codes solving the full Klein–Gordon equation in modified gravity are 1 per cent consistent (Winther et al. 2015) for $k \lesssim 7\,h\,{\rm Mpc}^{-1}$ in their prediction for the boost. These results are also consistent with the recent *Euclid* Collaboration code comparison project of Ref. Adamek et al. (2024), who also find 1 per cent consistency in the power spectrum boost in the nDGP and $f(R)$ gravity models among various codes that implement a full-field solver. This work also extends the number of full-field solvers considered, highlighting a great deal of consistency among the growing number of beyond-ΛCDM codes on the market.

We find that all approaches considered here are overall 2 per cent consistent with the benchmark N-body boost at scales $k \leq 1\,h\,{\rm Mpc}^{-1}$ and at $z \leq 1$. The only exceptions are `react` for the strongest modifications to ΛCDM and at $z = 0$. `mg-evolution` performs the best, with a general accuracy of 1 per cent at all scales considered ($k \leq 3\,h\,{\rm Mpc}^{-1}$), but this accuracy comes at the cost of tuning the screening parameter depending on the output redshift, modification strength, or resolution of the simulation, which might undermine the predictivity of the code. In Ref. Adamek et al. (2024) the authors further find a 3 per cent consistency between the COLA methods and

Table 4. Maximal per cent deviation of the non-linear matter power spectrum boost under various modelling approaches against benchmarks, at different redshifts for $k \leq 1(3)\,h\,\mathrm{Mpc}^{-1}$.

	Mg-evolution				COLA-FML			Hi-cola			React		
Model	$z = 0$	$z = 0.5$	$z = 1$	$z = 0$	$z = 0.5$	$z = 1$	$z = 0$	$z = 0.5$	$z = 1$	$z = 0$	$z = 0.5$	$z = 1$
N1	1(1) per cent	1(1) per cent	1(2) per cent	1(2) per cent	1(4) per cent	1(4) per cent	2(4) per cent	1(4) per cent	1(3) per cent	2(2) per cent	2(2) per cent	2(3) per cent
N5	1(1) per cent	1(1) per cent	1(1) per cent	1(1) per cent	1(1) per cent	1(1) per cent	1(1) per cent	1(1) per cent	1(1) per cent	1(1) per cent	1(1) per cent	1(1) per cent
CG	1(1) per cent	1(1) per cent	1(2) per cent	1(6) per cent	1(5) per cent	1(5) per cent	1(10) per cent	2(6) per cent	1(3) per cent	4(8) per cent	2(5) per cent	1(3) per cent
QCDM	1(5) per cent	1(3) per cent	1(2) per cent	–	–	–	2(6) per cent	1(3) per cent	1(3) per cent	1(1) per cent	1(4) per cent	1(5) per cent
K-mouflage A	–	–	–	–	–	–	1(4) per cent	1(3) per cent	1(3) per cent	2(17) per cent	1(8) per cent	1(4) per cent
K-mouflage B	–	–	–	–	–	–	1(2) per cent	1(1) per cent	1(1) per cent	2(10) per cent	1(5) per cent	1(2) per cent
K-mouflage C	–	–	–	–	–	–	1(1) per cent	1(1) per cent	1(1) per cent	1(4) per cent	1(3) per cent	1(1) per cent

the full-field solvers which is fairly consistent with our findings for nDGP, although we consider a slightly stronger modification which exhibits slightly stronger deviations from the `ecosmog` predictions.

We thus can advocate the safe use of these codes, and any emulators based upon them (see Carrion et al. 2024; Gordon et al. 2024; Tsedrik et al. 2024, , for example),[6] at fairly non-linear scales for scale-independent models. We note the caveat that emulation error should be quantified and appropriately accounted for.

For a more concrete estimate on the validity of these methods, we can consider a *Euclid*-like survey whose weak lensing analysis will have a signal-to-noise peaking at (conservatively) $z \approx 0.7$ (see Lepori et al. 2022, for example). Imposing a 2 per cent accuracy demand on the matter power spectrum model, and assuming a ΛCDM fiducial background cosmology, we can arguably trust all method predictions for $\ell_{\rm max} \lesssim 1800$. This roughly corresponds to the pessimistic scenario described in Ref. Blanchard et al. (2020).

At scales $k > 1\ h\,\mathrm{Mpc}^{-1}$ we find all codes begin to diverge by more than 2 per cent for the strongest modifications considered. They should thus not be used to model the highly non-linear scales of structure formation in the context of forthcoming LSS analyses without considering an appropriate theoretical error contribution to the error budget (see Audren et al. 2013, for example).

The goal of this work was to validate different methods to compute the non-linear matter power spectrum boost (see equation 32). This function inherently depends on the non-linear matter power spectrum of ΛCDM. This boost must be applied to an accurate ΛCDM spectrum prediction in order to get a non-linear modified matter power spectrum prediction. Therefore, the final modified gravity prescription inherits a dependence on predictions of ΛCDM. While we now have state-of-the-art high resolution tools to evaluate $P_{\rm NL}^{\Lambda\rm CDM}(k, z)$, the region in which these tools have internal accuracy within 1 per cent − 2 per cent may not be as broad as we need for extracting unbiased constraints on cosmological parameters for Stage-IV LSS surveys (see Gordon et al. 2024, for a more in depth discussion). Furthermore, it is expected that in beyond-ΛCDM analyses, extreme regions of the parameter space need to be sampled, which heightens the need for the development of more comprehensive emulators in ΛCDM.

In a similar vein, a further investigation of the impact of baryons in a full parameter inference scenario remains an imperative. It has been shown that the interplay between baryonic physics and cosmology exhibit some dependence at small scales (Elbers et al. 2024). However, it is unknown to what extent in the non-linear regime we can still extract relevant cosmological information, i.e. if we need to model baryonic physics deep inside the non-linear regime, $k \sim 10\ h\mathrm{Mpc}^{-1}$ or not. Alternatively to modelling baryonic physics at the level of the power spectrum, it would be interesting to investigate the performance of procedures that mitigate the impact of baryons in the parameter constrains, such as the methods described in Refs. Eifler et al. (2015) and Huang et al. (2019, 2021).

To conclude, let us highlight that the methods compared in this work have been designed with an element of theoretical flexibility in mind. There is a general shift to move beyond hard-coded codes designed to be valid for only one gravity model, and instead build more general tools that can be calibrated to a range of different

[6]The results of this work do not directly apply to the emulator produced in Ref. Fiorini et al. (2023), `ndgpemu`, as the screening approximation used to produced their training set is different from the ones adopted in this work.

models.[7] This is an essential step forward to streamline the testing of new theoretical ideas with data from Stage IV surveys.

ACKNOWLEDGEMENTS

The authors thank the anonymous referee for useful comments and feedback. BB is supported by a UKRI Stephen Hawking Fellowship (EP/W005654/2). ASG is supported by a STFC PhD studentship. FH acknowledges the Research Council of Norway and the resources provided by UNINETT Sigma2 – the National Infrastructure for High Performance Computing and Data Storage in Norway. FH is also supported by a grant from the Swiss National Supercomputing Centre (CSCS) under project ID s1051. TB is supported by ERC Starting Grant SHADE (grant no. StG 949572) and by a Royal Society University Research Fellowship (grant no. URF\R\231006). LA is supported by Fundação para a Ciência e a Tecnologia (FCT) through the research grants UIDB/04434/2020, UIDP/04434/2020 and from the FCT PhD fellowship grant with ref. number 2022.11152.BD. NF is supported by the Italian Ministry of University and Research (MUR) through the Rita Levi Montalcini project 'Tests of gravity on cosmic scales' with reference PGR19ILFGP. LA and NF also acknowledge the FCT project with ref. number PTDC/FIS-AST/0054/2021 and the COST Action CosmoVerse, CA21136, supported by COST (European Cooperation in Science and Technology). CH-A acknowledges support from the Excellence Cluster ORIGINS which is funded by the Deutsche Forschungsgemeinschaft (DFG, German Research Foundation) under Germany's Excellence Strategy – EXC-2094–390783311. GB is supported by the Alexander von Humboldt Foundation. BF is supported by a Royal Society Enhancement Award (grant no. RF\ERE\210304). This work used the DiRAC@Durham facility managed by the Institute for Computational Cosmology on behalf of the STFC DiRAC HPC Facility (www.dirac.ac.uk). The equipment was funded by BEIS capital funding via STFC capital grants ST/K00042X/1, ST/P002293/1, ST/R002371/1, and ST/S002502/1, Durham University, and STFC operations grant ST/R000832/1. DiRAC is part of the National e-Infrastructure. `Hi-cola` data was generated utilizing Queen Mary's Apocrita HPC facility, supported by QMUL Research-IT, and the Sciama High Performance Compute (HPC) cluster which is supported by the ICG, SEPNet and the University of Portsmouth. For the purpose of open access, the authors have applied a Creative Commons Attribution (CC BY) licence to any Author Accepted Manuscript version arising from this submission.

DATA AVAILABILITY

The halo model reaction software used in this article is publicly available in the `ACTio-Reactio` repository at https://github.com/nebblu/ACTio-ReACTio. In the same repository we also provide a `Mathematica` notebook, kmouflage.nb, which contains relevant calculations for the K-mouflage model. N-body matter power spectra measurements are available upon request.

REFERENCES

Abbott T. et al., 2016, MNRAS, 460, 1270
Abbott B. P. et al., 2017, ApJ, 848, L13
Adamek J., Daverio D., Durrer R., Kunz M., 2016a, J. Cosmol. Astropart. Phys., 2016, 053
Adamek J., Daverio D., Durrer R., Kunz M., 2016b, Nat. Phys., 12, 346
Adamek J. et al., 2024, Euclid preparation. Simulations and nonlinearities beyond Λ CDM. 1. Numerical methods and validation , preprint (arXiv:2409.03522)
Aghanim N. et al., 2020, A&A, 641, A6
Akeson R. et al., 2019, preprint (arXiv:1902.05569)
Alam S. et al., 2021, Phys. Rev. D, 103, 083533
Albrecht A. et al., 2006, preprint(astro-ph/0609591)
Albuquerque I. S., Frusciante N., Martinelli M., 2022, Phys. Rev. D, 105, 044056
Armendariz-Picon C., Damour T., Mukhanov V. F., 1999, Phys. Lett. B, 458, 209
Arnold C., Leo M., Li B., 2019, Nat. Astron., 3, 945
Arnold C., Li B., Giblin B., Harnois-Déraps J., Cai Y.-C., 2022, MNRAS, 515, 4161
Atayde L., Frusciante N., Bose B., Casas S., Li B., 2024, Phys. Rev. D, 110, 024082
Audren B., Lesgourgues J., Bird S., Haehnelt M. G., Viel M., 2013, J. Cosmol. Astropart. Phys., 2013, 026
Babichev E., Deffayet C., 2013, Class. Quantum Gravity, 30, 184001
Babichev E., Deffayet C., Ziour R., 2009, Int. J. Mod. Phys. D, 18, 2147
Bag S., Mishra S. S., Sahni V., 2018, Phys. Rev. D, 97, 123537
Baker T., Bellini E., Ferreira P. G., Lagos M., Noller J., Sawicki I., 2017, Phys. Rev. Lett., 119, 251301
Baker T., Clampitt J., Jain B., Trodden M., 2018, Phys. Rev. D, 98, 023511
Baker T. et al., 2022, J. Cosmol. Astropart. Phys., 2022, 031
Baker T., Barausse E., Chen A., de Rham C., Pieroni M., Tasinato G., 2023, J. Cosmol. Astropart. Phys., 2023, 044
Baldauf T., Mirbabayi M., Simonović M., Zaldarriaga M., 2016, preprint (arXiv:1602.00674)
Baldi M., Simpson F., 2015, MNRAS, 449, 2239
Barreira A., Li B., Baugh C. M., Pascoli S., 2012, Phys. Rev. D, 86, 124016
Barreira A., Li B., Hellwing W. A., Baugh C. M., Pascoli S., 2013a, J. Cosmol. Astropart. Phys., 2013, 027
Barreira A., Li B., Baugh C. M., Pascoli S., 2013b, J. Cosmol. Astropart. Phys., 2013, 056
Barreira A., Li B., Baugh C., Pascoli S., 2014, J. Cosmol. Astropart. Phys., 2014, 059
Barreira A., Brax P., Clesse S., Li B., Valageas P., 2015a, Phys. Rev. D, 91, 063528
Barreira A., Brax P., Clesse S., Li B., Valageas P., 2015b, Phys. Rev. D, 91, 123522
Barreira A., Sánchez A. G., Schmidt F., 2016, Phys. Rev. D, 94, 084022
Barroso J. A. A. et al., 2024, preprint (arXiv:2405.13491)
Battye R. A., Pace F., Trinh D., 2018, Phys. Rev. D, 98, 023504
Becker C., Arnold C., Li B., Heisenberg L., 2020, J. Cosmol. Astropart. Phys., 2020, 055
Belgacem E., Finke A., Frassino A., Maggiore M., 2019, J. Cosmol. Astropart. Phys., 2019, 035
Bellini E. et al., 2018, Phys. Rev. D, 97, 023520
Benevento G., Raveri M., Lazanu A., Bartolo N., Liguori M., Brax P., Valageas P., 2019, J. Cosmol. Astropart. Phys., 2019, 027
Bernardeau F., Colombi S., Gaztanaga E., Scoccimarro R., 2002, Phys. Rept., 367, 1
Bernardo H., Bose B., Franzmann G., Hagstotz S., He Y., Litsa A., Niedermann F., 2022, Universe, 2, 63
Blanchard A. et al., 2020, A&A, 642, A191
Bonici M. et al., 2023, A&A, 670, A47
Bose B., Koyama K., 2016, J. Cosmol. Astropart. Phys., 2016, 032
Bose B., Baldi M., Pourtsidou A., 2018, J. Cosmol. Astropart. Phys., 2018, 032
Bose B., Cataneo M., Tröster T., Xia Q., Heymans C., Lombriser L., 2020, MNRAS, 498, 4650
Bose B. et al., 2021, MNRAS, 508, 2479
Bose B., Tsedrik M., Kennedy J., Lombriser L., Pourtsidou A., Taylor A., 2023, MNRAS, 519, 4780

[7] A caveat here is that codes like `mg-glam` or `ecosmog` may always be needed for validation.

Brando G., Falciano F. T., Linder E. V., Velten H. E. S., 2019, J. Cosmol. Astropart. Phys., 2019, 018
Brando G., Fiorini B., Koyama K., Winther H. A., 2022, J. Cosmol. Astropart. Phys., 2022, 051
Brando G., Koyama K., Winther H. A., 2023, J. Cosmol. Astropart. Phys., 2023, 045
Brax P., Valageas P., 2014a, Phys. Rev. D, 90, 023507
Brax P., Valageas P., 2014b, Phys. Rev. D, 90, 023508
Brax P., van de Bruck C., Davis A.-C., Li B., Shaw D. J., 2011, Phys. Rev. D, 83, 104026
Brax P., Davis A.-C., Li B., Winther H. A., Zhao G.-B., 2013, J. Cosmol. Astropart. Phys., 2013, 029
Brax P., Rizzo L. A., Valageas P., 2015, Phys. Rev. D, 92, 043519
Brax P., Casas S., Desmond H., Elder B., 2021, Universe, 8, 11
Carrilho P., Carrion K., Bose B., Pourtsidou A., Hidalgo J. C., Lombriser L., Baldi M., 2022, MNRAS, 512, 3691
Carrion K., Carrilho P., Spurio Mancini A., Pourtsidou A., Hidalgo J. C., 2024, MNRAS, 532, 3914
Casas S. et al., 2023, preprint (arXiv:2306.11053)
Cataneo M., Lombriser L., Heymans C., Mead A., Barreira A., Bose S., Li B., 2019, MNRAS, 488, 2121
Cataneo M., Emberson J. D., Inman D., Harnois-Deraps J., Heymans C., 2020, MNRAS, 491, 3101
Catena R., Pietroni M., Scarabello L., 2007, Phys. Rev. D, 76, 084039
Chiba T., Yamaguchi M., 2013, J. Cosmol. Astropart. Phys., 2013, 040
Christiansen O., Hassani F., Jalilvand M., Mota D. F., 2023, J. Cosmol. Astropart. Phys., 2023, 009
Clifton T., Carrilho P., Fernandes P. G. S., Mulryne D. J., 2020, Phys. Rev. D, 102, 084005
Cooray A., Sheth R. K., 2002, Phys. Rept., 372, 1
Creminelli P., Vernizzi F., 2017, Phys. Rev. Lett., 119, 251302
Creminelli P., Lewandowski M., Tambalo G., Vernizzi F., 2018, J. Cosmol. Astropart. Phys., 2018, 025
Davis A.-C., Li B., Mota D. F., Winther H. A., 2012, ApJ, 748, 61
De Felice A., Tsujikawa S., 2012, J. Cosmol. Astropart. Phys., 02, 007
Deffayet C., Esposito-Farese G., Vikman A., 2009, Phys. Rev. D, 79, 084003
Deffayet C., Gao X., Steer D. A., Zahariade G., 2011, Phys. Rev. D, 84, 064039
Dvali G. R., Gabadadze G., Porrati M., 2000, Phys. Lett. B, 485, 208
Eifler T., Krause E., Dodelson S., Zentner A. R., Hearin A. P., Gnedin N. Y., 2015, MNRAS, 454, 2451
Elbers W. et al., 2024, preprint (arXiv:2403.12967)
Ezquiaga J. M., Zumalacárregui M., 2017, Phys. Rev. Lett., 119, 251304
Fiorini B., Koyama K., Baker T., 2023, J. Cosmol. Astropart. Phys., 2023, 045
Francfort J., Ghosh B., Durrer R., 2019, J. Cosmol. Astropart. Phys., 2019, 071
Frusciante N., Pace F., 2020, Phys. Dark Univ., 30, 100686
Frusciante N., Perenon L., 2020, Phys. Rept., 857, 1
Frusciante N., Peirone S., Atayde L., De Felice A., 2020, Phys. Rev. D, 101, 064001
Frusciante N. et al., 2024, A&A, 690, A133
Gabadadze G., Iglesias A., 2006, Phys. Lett. B, 639, 88
Giblin B., Cataneo M., Moews B., Heymans C., 2019, MNRAS, 490, 4826
Goldstein A. et al., 2017, ApJ, 848, L14
Gordon J., de Aguiar B. F., Rebouças J. a., Brando G., Falciano F., Miranda V., Koyama K., Winther H. A., 2024, Phys. Rev. D, 110, 083529
Gupta A. S., Fiorini B., Baker T., 2024, K-mouflage at high k: extending the reach of Hi-COLA, preprint (arXiv:2407.00855)
Harnois-Déraps J., Hernandez-Aguayo C., Cuesta-Lazaro C., Arnold C., Li B., Davies C. T., Cai Y.-C., 2023, MNRAS, 525, 6336
Harry I., Noller J., 2022, Gen. Relativ. Gravit., 54, 133
Hassani F., Lombriser L., 2020, MNRAS, 497, 1885
Hassani F., Adamek J., Kunz M., Vernizzi F., 2019, J. Cosmol. Astropart. Phys., 2019, 011
Hassani F., L'Huillier B., Shafieloo A., Kunz M., Adamek J., 2020, J. Cosmol. Astropart. Phys., 2020, 039
Hearin A. P., Zentner A. R., Ma Z., 2012, J. Cosmol. Astropart. Phys., 2012, 034
Hernández-Aguayo C., Arnold C., Li B., Baugh C. M., 2021, MNRAS, 503, 3867
Hernández-Aguayo C., Ruan C.-Z., Li B., Arnold C., Baugh C. M., Klypin A., Prada F., 2022, J. Cosmol. Astropart. Phys., 2022, 048
Hildebrandt H. et al., 2017, MNRAS, 465, 1454
Hinterbichler K., Khoury J., 2010, Phys. Rev. Lett., 104, 231301
Horndeski G. W., 1974, Int. J. Theor. Phys., 10, 363
Hou J., Bautista J., Berti M., Cuesta-Lazaro C., Hernández-Aguayo C., Tröster T., Zheng J., 2023, Universe, 9, 302
Howlett C., Manera M., Percival W. J., 2015, Astron. Comput., 12, 109
Hu W., Sawicki I., 2007, Phys.Rev., D76, 064004
Hu B., Raveri M., Frusciante N., Silvestri A., 2014, Phys. Rev. D, 89, 103530
Huang H.-J., Eifler T., Mandelbaum R., Dodelson S., 2019, MNRAS, 488, 1652
Huang H.-J. et al., 2021, MNRAS, 502, 6010
Ivezić v. et al., 2019, ApJ, 873, 111
Jain B., Khoury J., 2010, Ann. Phys., 325, 1479
Jing Y. P., 2005, ApJ, 620, 559
Kable J. A., Benevento G., Frusciante N., De Felice A., Tsujikawa S., 2022, J. Cosmol. Astropart. Phys., 2022, 002
Khoury J., Weltman A., 2004, Phys. Rev. Lett., 93, 171104
Khoury J., Wyman M., 2009, Phys. Rev. D, 80, 064023
Kimura R., Kobayashi T., Yamamoto K., 2012, Phys. Rev. D, 85, 024023
Klypin A., Prada F., 2018, MNRAS, 478, 4602
Knabenhans M. et al., 2019, MNRAS, 484, 5509
Kobayashi T., 2019, Rept. Prog. Phys., 82, 086901
Kobayashi T., Yamaguchi M., Yokoyama J., 2010, Phys. Rev. Lett., 105, 231302
Koyama K., Maartens R., 2006, J. Cosmol. Astropart. Phys., 2006, 016
LSST Dark Energy Science Collaboration, 2012, preprint (arXiv:1211.0310)
Lepori F. et al., 2022, A&A, 662, A93
Levi M. et al., 2019, Bulletin of the American Astronomical Society, 51, 57, preprint (arXiv:1907.10688)
Li B., Zhao G.-B., Teyssier R., Koyama K., 2012, J. Cosmol. Astropart. Phys., 2012, 051
Li B., Zhao G.-B., Koyama K., 2013a, J. Cosmol. Astropart. Phys., 2013, 023
Li B., Barreira A., Baugh C. M., Hellwing W. A., Koyama K., Pascoli S., Zhao G.-B., 2013b, J. Cosmol. Astropart. Phys., 2013, 012
Llinares C., Mota D. F., Winther H. A., 2014, A&A, 562, A78
Lombriser L., 2016, J. Cosmol. Astropart. Phys., 2016, 039
Lombriser L., Lima N. A., 2017, Phys. Lett., 765, 382
Lombriser L., Taylor A., 2016, J. Cosmol. Astropart. Phys., 2016, 031
Lombriser L., Hu W., Fang W., Seljak U., 2009, Phys. Rev. D, 80, 063536
Lue A., 2006, Phys. Rept., 423, 1
Luty M. A., Porrati M., Rattazzi R., 2003, J. High Energy Phys., 2003, 029
Martinelli M. et al., 2021, A&A, 649, A100
Mead A., Heymans C., Lombriser L., Peacock J., Steele O., Winther H., 2016, MNRAS, 459, 1468
Mead A., Brieden S., Tröster T., Heymans C., 2021, MNRAS, 502, 1401
Nicolis A., Rattazzi R., Trincherini E., 2009, Phys. Rev. D, 79, 064036
Nouri-Zonoz A. R., Hassani F., Kunz M., 2024, preprint (arXiv:2405.10424)
Pace F., Battye R., Bellini E., Lombriser L., Vernizzi F., Bolliet B., 2021, J. Cosmol. Astropart. Phys., 2021, 017
Peirone S., Frusciante N., Hu B., Raveri M., Silvestri A., 2018, Phys. Rev. D, 97, 063518
Peirone S., Benevento G., Frusciante N., Tsujikawa S., 2019, Phys. Rev. D, 100, 063540
Perlmutter S. et al., 1999, ApJ, 517, 565
Piga L., Marinucci M., D'Amico G., Pietroni M., Vernizzi F., Wright B. S., 2023, J. Cosmol. Astropart. Phys., 2023, 038
Prunet S., Pichon C., Aubert D., Pogosyan D., Teyssier R., Gottloeber S., 2008, ApJS, 178, 179
Puchwein E., Baldi M., Springel V., 2013, MNRAS, 436, 348
Quartin M., Tsujikawa S., Amendola L., Sturani R., 2023, J. Cosmol. Astropart. Phys., 2023, 049

Ramachandra N., Valogiannis G., Ishak M., Heitmann K., 2021, Phys. Rev. D, 103, 123525
Renk J., Zumalacárregui M., Montanari F., Barreira A., 2017, J. Cosmol. Astropart. Phys., 2017, 020
de Rham C., Melville S., 2018, Phys. Rev. Lett., 121, 221101
de Rham C., Melville S., Noller J., 2021, J. Cosmol. Astropart. Phys., 2021, 018
Riess A. G. et al., 1998, AJ, 116, 1009
Ruan C.-Z., Hernández-Aguayo C., Li B., Arnold C., Baugh C. M., Klypin A., Prada F., 2022, J. Cosmol. Astropart. Phys., 2022, 018
Sakstein J., Jain B., 2017, Phys. Rev. Lett., 119, 251303
Sawicki I., Bellini E., 2015, Phys. Rev. D, 92, 084061
Schmidt F., 2009a, Phys. Rev. D, 80, 043001
Schmidt F., 2009b, Phys. Rev. D, 80, 123003
Schmidt F., Hu W., Lima M., 2010, Phys. Rev. D, 81, 063005
Scoccimarro R., 2009, Phys. Rev. D, 80, 104006
Sefusatti E., Crocce M., Scoccimarro R., Couchman H., 2016, MNRAS, 460, 3624
Simpson F., 2010, Phys. Rev. D, 82, 083505
Srinivasan S., Thomas D. B., Pace F., Battye R., 2021, J. Cosmol. Astropart. Phys., 2021, 016
Srinivasan S., Thomas D. B., Battye R., 2024, J. Cosmol. Astropart. Phys., 2024, 039
Takahashi R., Sato M., Nishimichi T., Taruya A., Oguri M., 2012, ApJ, 761, 152
Tassev S., Zaldarriaga M., Eisenstein D., 2013, J. Cosmol. Astropart. Phys., 2013, 036
Teyssier R., 2002, A&A, 385, 337
Tsedrik M., Bose B., Carrilho P., Pourtsidou A., Pamuk S., Casas S., Lesgourgues J., 2024, JCAP, 10, 099
Vainshtein A., 1972, Phys.Lett., 39, 393
Valogiannis G., Bean R., 2017, Phys. Rev. D, 95, 103515
Will C. M., 2014, Living Rev. Rel., 17, 4
Winther H. A., Ferreira P. G., 2015a, Phys. Rev. D, 91, 123507
Winther H. A., Ferreira P. G., 2015b, Phys. Rev. D, 92, 064005
Winther H. A. et al., 2015, MNRAS, 454, 4208
Winther H. A., Koyama K., Manera M., Wright B. S., Zhao G.-B., 2017, J. Cosmol. Astropart. Phys., 2017, 006
Wright B. S., Sen Gupta A., Baker T., Valogiannis G., Fiorini B., 2023, J. Cosmol. Astropart. Phys., 2023, 040
Zhao G.-B., 2014, ApJ, 211, 23
Zumalacárregui M., Bellini E., Sawicki I., Lesgourgues J., Ferreira P. G., 2017, J. Cosmol. Astropart. Phys., 2017, 019

APPENDIX A: K-MOUFLAGE REACT PATCH

Here we present the expressions needed to calculate the halo model reaction (see equation 27) in the K-mouflage model. The halo model reaction relies on both the halo model (see Cooray & Sheth 2002, for a review) and 1-loop perturbation theory (see Bernardeau et al. 2002, for a review). In particular, besides the background expansion $H(a)$, we require the modifications to the 1st, 2nd, 3rd order perturbative and non-linear Poisson equations, as well as contributions to the potential energy of haloes in order to solve the virial theorem (see Cataneo et al. 2019; Bose et al. 2020, for more details). K-mouflage also comes with a friction term correction to the Euler equation (Brax & Valageas 2014b).

A1 Background

For the background expansion we must solve the Klein–Gordon and Friedmann equations simultaneously. We do this numerically in `react` as done in Ref. Hernández-Aguayo et al. (2022). The Friedmann equations are

$$\frac{\mathcal{H}^2}{H_0^2}\left[1-\frac{\varphi'^2}{6}\right] = \frac{A(\varphi)\Omega_{\rm m,0}}{a} + \frac{1}{3}\lambda^2 a^2 + \frac{(2n-1)}{3}\lambda^2 a^2 K_0\left(\frac{\varphi'^2}{2\lambda^2 a^2}\right)^n \frac{\mathcal{H}^{2n}}{H_0^{2n}}, \tag{A1}$$

$$\frac{\mathrm{d}\mathcal{H}}{\mathrm{d}\tau}\frac{1}{H_0^2} = -\frac{A(\varphi)\Omega_{\rm m,0}}{2a} + \frac{1}{3}\lambda^2 a^2 - \frac{1}{3}\varphi'^2\frac{\mathcal{H}^2}{H_0^2} - \frac{(n+1)}{3}\lambda^2 a^2 K_0\left(\frac{\varphi'^2}{2\lambda^2 a^2}\right)^n \frac{\mathcal{H}^{2n}}{H_0^{2n}}, \tag{A2}$$

while the Klein–Gordon equation is given as

$$(K_X + 2\bar{X}K_{XX})\left[\frac{\mathcal{H}^2}{H_0^2}\varphi'' + \frac{\mathrm{d}\mathcal{H}}{\mathrm{d}\tau}\frac{1}{H_0^2}\varphi'\right] + 2(K_X - \bar{X}K_{XX})\frac{\mathcal{H}^2}{H_0^2}\varphi' + 3\frac{\mathrm{d}A(\varphi)}{\mathrm{d}\varphi}\frac{\Omega_{\rm m,0}}{a} = 0, \tag{A3}$$

where $K_{XX} = \mathrm{d}^2K/\mathrm{d}X^2$ and we recall primes denote derivatives with respect to $\ln a$. In these equations we have defined the normalized scalar field $\varphi \equiv \phi/M_{\rm pl}$ and used the conformal Hubble rate $\mathcal{H}(a) = H(a)a$. τ is conformal time. We indicate that a few typographical errors did occur in Ref. Hernández-Aguayo et al. (2022) which have been corrected in the above equations.

To solve these equations we first find the analytic solutions to equation (A1) for a given value of n.[8] For $n = 2$ this is a quadratic equation in $\mathcal{H}^2/H_0^2$. Then, for a given value of a (or $\ln a$) we can substitute $\mathcal{H}$ and equation (A2) in equation (A3), enabling us to solve for the entire evolution of φ (and φ'), and consequently $H(a)$.

A2 Perturbations

The linear modification to the Poisson equation is given by (Brax & Valageas 2014b)

$$\frac{G_{\rm eff,L}}{G_{\rm N}} = A(\varphi)\left(1 + \frac{2\beta_{\rm K}^2}{K_X}\right). \tag{A4}$$

Here we have included the conformal factor $A(\varphi)$, that comes along with $\rho_{\rm m}$ in the Poisson equation, equation (4). Note that $G_{\rm eff,L}/G_{\rm N} = \mu(k,a)$ in the `react` standard notation of Refs. Bose & Koyama (2016), Cataneo et al. (2019), and Bose et al. (2020, 2023) for example.

The second and third-order symmetrized modifications to the Poisson equation, in the same notation of Ref. Bose & Koyama (2016) and Bose et al. (2020), are (Brax & Valageas 2014b)

$$\gamma_2(\boldsymbol{k}_1, \boldsymbol{k}_2, a) = 0,$$

$$\gamma_3(\boldsymbol{k}_1, \boldsymbol{k}_2, \boldsymbol{k}_3, a) = -\frac{9}{2}K_{XX}\left(\frac{A(\varphi)\Omega_{\rm m,0}}{a}\frac{H_0^2}{\mathcal{H}^2}\right)^3\left(\frac{\beta_{\rm K}}{K_X}\right)^4\frac{\mathcal{H}^4}{H_0^2}\frac{1}{a^2\lambda^2} \times\left[\frac{(\mu_{12}+2\mu_{13}\mu_{23})}{k_1k_2} + \frac{(\mu_{13}+2\mu_{23}\mu_{12})}{k_1k_3} + \frac{(\mu_{23}+2\mu_{13}\mu_{12})}{k_2k_3}\right], \tag{A5}$$

where we have defined $\mu_{ij} \equiv \hat{k}_i \cdot \hat{k}_j$ and $k_i = |\boldsymbol{k}_i|$.

Lastly, we also have a modification to the Euler equation in the form of a friction term (Brax & Valageas 2014b). Similar terms have been included in `react` in the context of interacting dark energy models (Simpson 2010; Baldi & Simpson 2015; Bose, Baldi &

[8] We provide a Mathematica notebook which computes the solutions for $n = 2, 3$ and checks consistency of the equations.

Pourtsidou 2018; Carrilho et al. 2022). In the K-mouflage model considered here, this term is given as

$$A_{\rm friction} = \beta_{\rm K}\varphi' \,. \tag{A6}$$

This term enters the Euler equation as expressed in equation (2.10) of Ref. Bose et al. (2018) for example.

A3 Spherical collapse

The halo model reaction also requires us to solve for the spherical top-hat overdensity. This involves solving the evolution equation for the top-hat radius which requires specification of the non-linear Poisson equation. The modification to this equation is to a good approximation equal to the linear modification at extra galactic scales given the smallness of the K-mouflage radius (Brax & Valageas 2014b)

$$\frac{G_{\rm eff}(k,a)}{G_{\rm N}} = \frac{G_{\rm eff,\,L}(a)}{G_{\rm N}} \,. \tag{A7}$$

We note in the notation of Ref. Cataneo et al. (2019), $\mathcal{F} = G_{\rm eff}/G_{\rm N} - 1 = \Delta G_{\rm eff}/G_{\rm N}$. In `reactF` appears as $1+\mathcal{F}$ in the Poisson equation. This yields the correct conformal factor accounting for the Einstein-frame transformation of the background density in the non-linear Poisson equation, as it is already explicit in equation (A4).

Lastly, we note that the top-hat radius evolution also must include the friction term equation (A6).

A4 Virial theorem

Here we present the potential energy contributions to the virial theorem in the K-mouflage model considered. This is needed to calculate the virial mass in the halo model reaction calculations. The specific components we require are (Schmidt, Hu & Lima 2010; Cataneo et al. 2019)

$$\frac{W_{\rm N}}{E_0} = -\Omega_{\rm m,0}\tfrac{a^{-1}}{a_{\rm i}^2} y^2(1+\delta)\,; \tag{A8}$$

$$\frac{W_{\phi}}{E_0} = -\Omega_{\rm m,0}\mathcal{F}\tfrac{a^{-1}}{a_{\rm i}^2} y^2\delta\,; \tag{A9}$$

$$\frac{W_{\rm eff}}{E_0} = -\tfrac{1}{3M_{\rm pl}^2H_0^2}(1+3w_{\rm eff})\,\bar{\rho}_{\rm eff}\tfrac{a^2}{a_{\rm i}^2} y^2\,; \tag{A10}$$

$$\frac{W_{\rm fric}}{E_0} = -2A_{\rm friction}\tfrac{H^2}{H_0^2}\tfrac{a^2}{a_{\rm i}^2}\, y\, y'\,, \tag{A11}$$

where $y \equiv \frac{R_{\rm TH}}{R_{\rm i}}\frac{a_{\rm i}}{a}$, $R_{\rm TH}$ being the comoving top-hat radius, $R_{\rm i}$ the initial top-hat radius, and E_0 is a normalization. These represent the Newtonian contribution, the scalar field contribution, the effective dark energy contribution, and a frictional force contribution as derived in Ref. Carrilho et al. (2022). In the K-mouflage model the scalar field affects both force enhancement and acts as an effective dark energy component.

We recall that $\mathcal{F} = G_{\rm eff}/G_{\rm N} - 1$ which does not account for the correct conformal factor to appear in equation (A9) in the K-mouflage model. In this case we should have

$$\begin{aligned}\frac{W_{\phi}}{E_0} &= -\Omega_{\rm m,0}\left[G_{\rm eff,L}/G_{\rm N} - A(\varphi)\right]\frac{a^{-1}}{a_{\rm i}^2} y^2\delta\,,\\ &= -\Omega_{\rm m,0}\left[A(\varphi)\frac{2\beta_{\rm K}^2}{K_X}\right]\frac{a^{-1}}{a_{\rm i}^2} y^2\delta\,,\end{aligned} \tag{A12}$$

where we used equation (A7) and equation (A4). $A_{\rm friction}$ is given by equation (A6). $w_{\rm eff} = \bar{p}_{\rm eff}/\bar{\rho}_{\rm eff}$ and $\bar{\rho}_{\rm eff}$ are the equation of state and energy density of the effective dark energy fluid component, with $\bar{p}_{\rm eff}$ being the fluid's pressure. These are given in the Einstein frame by (Brax & Valageas 2014a, b):

$$\bar{\rho}_{\rm eff} = -M_{\rm pl}^2H_0^2\lambda^2(K - M_{\rm pl}^2H^2\bar{\phi}'^2K_X)\,; \tag{A13}$$

$$\bar{p}_{\rm eff} = M_{\rm pl}^2H_0^2\lambda^2K\,. \tag{A14}$$

We then get

$$w_{\rm eff} = -\frac{K}{K - M_{\rm pl}^2H^2\bar{\phi}'^2K_X}\,. \tag{A15}$$

We can simplify equation (A10) further by noting that when adopting the model in equation (14) we have

$$K_X = \frac{1}{H_0^2\lambda^2M_{\rm pl}^2} + K_0\frac{1}{H_0^{2n}\lambda^{2n}M_{\rm pl}^{2n}} n\, X^{n-1}\,. \tag{A16}$$

Substituting this into equation (A15), we find the effective dark energy contribution to the potential energy is given by

$$\frac{W_{\rm eff}}{E_0} = -\frac{\lambda^2}{3}\left[2K + \frac{H^2}{H_0^2}\frac{\varphi'^2}{\lambda^2}\left(1 + K_0nX^{n-1}\right)\right]\frac{a^2}{a_{\rm i}^2}y^2\,. \tag{A17}$$

Finally, we should note that the Newtonian contribution also should have a conformal factor along with $\Omega_{\rm m,0}$

$$\frac{W_{\rm N}}{E_0} = -A(\varphi)\Omega_{\rm m,0}\frac{a^{-1}}{a_{\rm i}^2}y^2(1+\delta)\,. \tag{A18}$$

APPENDIX B: PARAMETRIZED POST-FRIEDMANNIAN EXPRESSIONS

Here we review expressions for the general parametrization of the effective gravitational constant appearing in the non-linear Poisson equation as described in Ref. Lombriser (2016). This is based on the parametrized post-Friedmannian framework and is the means of modelling modifications to non-linear structure formation in the `mg-evolution` code. This parametrization has also been implemented in the `react` code (Bose et al. 2023).

`mg-evolution` adopts a generalized form of the Vainshtein screening effect given by (Lombriser 2016)

$$\frac{\Delta G_{\rm eff,\,NL}}{G} = b\left(\frac{k_*}{k}\right)^{a_f}\left\{\left[1+\left(\frac{k}{k_*}\right)^{a_f}\right]^{1/b} - 1\right\}, \tag{B1}$$

where NL stands for non-linear, and k_* and b, respectively, characterize the effective screening wavenumber and the interpolation rate between the screened and unscreened regimes. This expression augments the linear theory prediction as given in equation (22) to give the full solution for $G_{\rm eff}$. We shall briefly provide the particular form of this expression for the three models considered in this work and refer the reader to Ref. Lombriser (2016) for more details.

B1 nDGP

To parametrize nDGP gravity we consider (see Lombriser 2016)

$$\frac{\Delta G_{\rm nDGP,NL}}{G_{\rm N}} = \frac{1}{3\beta(a)}\left(\frac{k_*}{k}\right)^3\left\{\left[1+\left(\frac{k}{k_*}\right)^3\right]^{\frac{1}{2}} - 1\right\}, \tag{B2}$$

where k_* corresponds approximately to the Vainshtein radius:

$$r_* = \frac{16\pi G_{\rm N}\delta M r_c^2}{9\beta^2}, \tag{B3}$$

where δM is the mass enclosed by a spherical region, r_c is the crossover scale in nDGP theories, and $\beta(a)$ is given below. The Vainshtein radius effectively defines a region where the fifth force introduced by the scalar field gets shielded. The effective screening wavenumber k_* can in principle be modelled. However, it is treated as a free parameter in `mg-evolution`. The function $\beta(a)$ reads as

$$\beta(a) = 1 + 2Hr_c\left(1 + \frac{\dot{H}}{3H^2}\right), \tag{B4}$$

and the linear effective gravitational constant in nDGP is given by

$$\frac{G_{\rm eff,\,L}}{G_{\rm N}} = 1 + \frac{1}{3\beta(a)}. \tag{B5}$$

We remind the reader that a cosmological background that matches that of ΛCDM is assumed.

B2 Cubic Galileon

To parametrize the Cubic Galileon we adopt equation (22), with the nonlinear parametrization

$$\frac{\Delta G_{\rm CG,\,NL}}{G_{\rm N}} = \left(\frac{k_*}{k}\right)^3 \left\{\left[1 + \left(\frac{k}{k_*}\right)^3\right]^{\frac{1}{2}} - 1\right\}. \tag{B6}$$

To obtain the linear regime parametrization we use the effective gravitational potential in Cubic Galileon theory in the linear regime, which reads as (Barreira et al. 2013a)

$$\frac{\Delta G_{\rm CG,\,L}}{G_{\rm N}} = -\frac{2}{3}\frac{c_3\dot{\phi}^2}{M_{\rm pl}\mathcal{M}^3\beta_2}, \tag{B7}$$

where ϕ is the Galileon scalar field. β_2 and $\mathcal{M}^3$ read,

$$\beta_2 \equiv 2\frac{\mathcal{M}^3 M_{\rm pl}}{\dot{\phi}^2}\beta_1, \tag{B8}$$

$$\mathcal{M}^3 \equiv M_{\rm pl}H_0^2, \tag{B9}$$

where

$$\beta_1 \equiv \frac{1}{6c_3}\left[-c_2 - \frac{4c_3}{\mathcal{M}^3}(\ddot{\phi} + 2H\dot{\phi}) + 2\frac{c_3^2}{M_{\rm pl}^2\mathcal{M}^6}\dot{\phi}^4\right]. \tag{B10}$$

We consider $c_2 = -1$ and we use the tracker solution (Bellini et al. 2018),

$$\xi \equiv \frac{\dot{\phi}H}{M_{\rm pl}H_0^2}, \tag{B11}$$

where ξ is a constant and can be written in terms of c_2, c_3,

$$\xi = -\frac{c_2}{6c_3} = \frac{1}{6c_3}. \tag{B12}$$

As a result, we have the following solutions for $\dot{\phi}$ and $\ddot{\phi}$

$$\dot{\phi} = \frac{\xi M_{\rm pl}H_0^2}{H}, \quad \ddot{\phi} = -\frac{\xi M_{\rm pl}H_0^2\dot{H}}{H^2}. \tag{B13}$$

Following the discussion presented in Ref. Barreira et al. (2013b) for the background tracker solution, we can derive the Hubble expansion rate as a function of scale factor

$$\frac{H^2}{H_0^2} = \frac{1}{2}\Big[\left(\Omega_{\rm m,0}a^{-3} + \Omega_{\rm r,0}a^{-4}\right) + \sqrt{\left(\Omega_{\rm m,0}a^{-3} + \Omega_{\rm r,0}a^{-4}\right)^2 + 4\left(1 - \Omega_{\rm m,0} - \Omega_{\rm r,0}\right)}\Big], \tag{B14}$$

where $H_0^2 = \frac{8\pi G}{3}$ in `mg-evolution` units and $\Omega_{\rm r,0}$ is the radiation energy density fraction today. Computing the cosmic time derivative results in,

$$\frac{\dot{H} + H^2}{H_0^2} = -\frac{(a\Omega_{\rm m,0} + 2\Omega_{\rm r,0})}{4a^2} - \frac{(a\Omega_{\rm m,0} + \Omega_{\rm r,0})(3a\Omega_{\rm m,0} + 4\Omega_{\rm r,0})}{4a^6\sqrt{4(1 - \Omega_{\rm m,0} - \Omega_{\rm r,0}) + \frac{(a\Omega_{\rm m,0} + \Omega_{\rm r,0})^2}{a^8}}} + \frac{a^2}{2}\sqrt{4(1 - \Omega_{\rm m,0} - \Omega_{\rm r,0}) + \frac{(a\Omega_{\rm m,0} + \Omega_{\rm r,0})^2}{a^8}}.$$

B3 K-mouflage

Here we derive the effective gravitational constant appearing in the non-linear Poisson equation for the K-mouflage model described in Section 2.3. We follow Ref. Lombriser (2016). We also note that a conformal factor, $A(\varphi)$, still needs to be applied to transform the density appearing in the non-linear Poisson equation which is not included in the $G_{\rm KM,eff}$ expressions below.

The effective modification assuming a spherically symmetric matter distribution is given as (Brax & Valageas 2014b; Winther & Ferreira 2015a)

$$\frac{\Delta G_{\rm KM,eff}}{G_{\rm N}} = \frac{2\,\beta_{\rm K}^2}{K_X H_0^2\lambda^2 M_{\rm pl}^2}. \tag{B15}$$

Using the Klein–Gordon equation for a spherically symmetric matter distribution we can write K_X as

$$K_X^2 X = -\frac{2\,\beta_{\rm K}^2}{H_0^4\lambda^4 M_{\rm pl}^2}F_{\rm N}^2, \tag{B16}$$

where the Newtonian force is just $F_{\rm N} = G_{\rm N}M(<r)/r^2$, r being the physical radial coordinate and $M(<r)$ being the mass enclosed in radius r. Substituting for K_X in equation (B15) gives

$$\frac{\Delta G_{\rm KM,eff}}{G_{\rm N}} = \frac{\beta_{\rm K}}{M_{\rm pl}}\frac{1}{F_{\rm N}}\sqrt{-2X}. \tag{B17}$$

Now to solve for X we can adopt the model in equation (14). By using equation (A16) to solve equation (B16) we get

$$X = \frac{H_0^2\lambda^2 M_{\rm pl}^2}{6K_0}\frac{[1 - f(x)]^2}{f(x)}, \tag{B18}$$

where

$$f(x) = \left(1 + x + \sqrt{x(x+2)}\right)^{\frac{1}{3}}, \tag{B19}$$

and we have defined $x \equiv -C_A/r^4$, C_A being a parameter proportional to K_0, defined as

$$C_A \equiv \frac{54\beta_{\rm K}^2 G_{\rm N}^2 M^2}{H_0^2\lambda^2}K_0. \tag{B20}$$

We have written $M = M(<r)$ for compactness. It should be pointed out that $x \in (-2, 0)$ yields no solution for X which can be a problem for very large r and $K_0 > 0$. This will not generally be an issue as we look for solutions in the non-linear regime.

Substituting equation (B18) into equation (B17) gives

$$\frac{\Delta G_{\rm KM,eff}}{G_{\rm N}} = C_B\frac{1 - f(x)}{\sqrt{xf(x)}}, \tag{B21}$$

where

$$C_B \equiv 3\sqrt{2}\beta_{\rm K}^2. \tag{B22}$$

We note that in Ref. Lombriser (2016) there seems to be a missing factor of $1/(2\sqrt{2})$ in equation (3.26) in order to have the identification

$C_A = C_2^2$. We allow here the case when $x \leq 0$ which can occur for $K_0 > 0$. Further, we note $C_1 = -C_B$, C_1 and C_2 being the equivalent quantities for C_A and C_B in Ref. Lombriser (2016). We include a Mathematica notebook with our derivations.

We now derive the PPF expression from the limits of equation (B21):

$$\frac{\Delta G_{\rm KM,eff}}{G_{\rm N}} \to 2\beta_{\rm K}^2 \qquad \text{for} \qquad |x| \ll 1 \ (\text{i.e.}\, r^4 \gg |C_A|)\,, \tag{B23}$$

$$\frac{\Delta G_{\rm KM,eff}}{G_{\rm N}} \to \frac{C_B r^{4/3}}{(-C_A)^{1/3}} \qquad \text{for} \qquad |x| \gg 1 \ (\text{i.e.}\, r^4 \ll |C_A|)\,, \tag{B24}$$

which are the same limits obtained by Ref. Lombriser (2016).

We now map these onto the (real space) PPF expression, equation (5.3) of Ref. Lombriser (2016)

$$\frac{\Delta G_{\rm eff}}{G_{\rm N}} = p_1 p_2 \frac{(1+s^{a_f})^{\frac{1}{p_1}} - 1}{s^{a_f}}\,, \tag{B25}$$

where

$$a_f = \frac{p_1}{p_1 - 1} p_3\,, \tag{B26}$$

and $s = y_{\rm scr}/y_{\rm h}$. y is the normalized top-hat radius

$$y \equiv \frac{R_{\rm TH}/a}{R_i/a_i}\,. \tag{B27}$$

$R_{\rm TH}$ and R_i are the comoving halo top-hat radius and a_i the initial scale factor. The dimensionless screening scale is given by

$$y_{\rm scr} = p_4 a^{p_5} (2G_{\rm N} H_0 M_{\rm vir})^{p_6} \left(\frac{y_{\rm env}}{y_{\rm h}}\right)^{p_7}\,. \tag{B28}$$

$y_{\rm env}$ refers to the normalized radius of the environment and $M_{\rm vir}$ is the virial mass of the halo.

Comparing equation (B25) and equation (B28) with equation (B23) and equation (B24) we find, for a choice of p_1,

$$\begin{aligned} p_2 &= \frac{2\beta_{\rm K}^2}{p_1}, \qquad p_3 = \frac{4}{3}\frac{p_1 - 1}{p_1}, \\ p_4 &= \left[\frac{-\sqrt{2}K_0 p_1^3 \beta_{\rm K}^2}{\lambda^2}\right]^{\frac{1}{4}} \Omega_{\rm m,0}^{\frac{1}{3}}, \\ p_5 &= -1, \qquad p_6 = 1/6, \qquad p_7 = 0\,. \end{aligned} \tag{B29}$$

We note that whether there's a p_1 in p_3 depends on whether p_1 is positive or negative (see equation 2.14 of Ref. Lombriser 2016). We have also used $M_{\rm vir} \approx 4\pi\,\Omega_{\rm m,0}\rho_{\rm crit} R_{\rm th}^3/3$.

This paper has been typeset from a TEX/LATEX file prepared by the author.